The effect of the operational environment on the survivability of passenger ships

Mauro, Francesco; Vassalos, Dracos

Important note
To cite this publication, please use the final published version (if applicable).
Please check the document version above.

The effect of the operational environment on the survivability of passenger ships

Francesco Mauro [a,b,*], Dracos Vassalos [a,c]

[a] *The Maritime Safety Research Centre, Department of Naval Architecture, Ocean and Marine Engineering (NAOME), University of Strathclyde, 100 Montrose St., Glasgow, G4 0LZ, Scotland, UK*
[b] *Department of Maritime and Transport Technology, Faculty of Mechanical, Maritime and Materials Engineering, Delft University of Technology, Leeghwaterstraat 17, 2628 CA, Delft, The Netherlands*
[c] *Sharjah Maritime Academy, 180018, Khorfakkan, Sharjah, United Arab Emirates*

ARTICLE INFO

ABSTRACT

The in-force probabilistic framework for passenger ship survivability assessment covers collision hazards. The framework primarily pertains to a static approach. Nonetheless, more complex dynamic analyses usually employ the same damage definitions, adding besides the breach characteristics, the environmental condition selection or, more precisely, the irregular wave environment necessary to simulate the damage scenarios. The traditional dynamic approaches to survivability consider only the significant wave height sampled from statistical formulations, with the wave period deriving from a constant steepness assumption. However, wave height and period influence ship dynamics in waves differently, especially concerning survivability after damage. Therefore, aiming at a direct assessment of ship survivability and the probability of loss of lives determination in realistic operational scenarios, it is essential to properly study the influence of combined variations of wave height and periods and their occurrence. The present study proposes a methodology for dynamic simulations in site-specific conditions derived from the Global Wave Statistics. The study documents the process in two critical collision damages for a reference passenger ship, using wave height and period combinations typical of the main sea areas of interest for passenger ships and performing a sensitivity analysis on the simulations needed to evaluate survivability. This enhanced analysis allows identifying the limiting environmental conditions for the critical damage cases, including the effect of heading variations, determining the ship's survivability to specific damage in an operational area.

1. Introduction

Damage stability for passenger ships has widely developed as a subject over the last 60 years (Papanikolaou, 2007; Manderbacka et al., 2019), reaching the most relevant scientific advances during the past two decades. Therefore, damage stability and, in particular, the study of survivability after an accident is an integral part of the design process of modern passenger ships, providing a life/cycle flooding risk management for the vessel (Vassalos, 2022). As a consequence, the survivability of a passenger ship is a relevant attribute for the design of new vessels (Atzampos, 2019; Papanikolaou et al., 2013; Vanem et al., 2007). However, the application of damage stability study has been mainly oriented to simplified static approaches, easily usable by designers and directly linked to in-force regulations (IMO, 2009, 2020). Moreover, with the rising complexity of passenger ship internal layout, static calculations may deviate from a proper representation

of the physical phenomena associated with flooding (Santos et al., 2002; Ruponen et al., 2022a), especially in an irregular-sea environment (Spanos and Papanikolaou, 2012). It is then essential giving more importance to the first principle-based tools for vessel survivability during the design process of a passenger ship (Vassalos, 2016).

The assessment of damage stability with direct calculations requires modelling complicated phenomena related to the coupling between ship motions and the dynamic process of floodwater as well as its interaction with the ship and the wave environment. In that respect, the probabilistic framework considers the irregular wave environment by giving importance to the significant wave height H_s only, deriving formulations from statistics of accidents (IMO, 2009; Jasionowski, 2009) or generic worldwide statistics in open seas (Luhmann et al., 2018). The modelling of the wave period (either the peak period T_p or zero-crossing period T_z) directly derives from the application of one parameter wave

---

spectra or from the assumption of modelling irregular waves with a constant slope. However, the wave period is also influencing the ship dynamics in waves, both in intact and damaged conditions. Another assumption intrinsic in statutory regulations and practical guidelines for dynamic simulations is the evaluation of damage stability assessment in beam seas, considering waves impacting the damaged side. A limited number of studies in the literature address the variations of survivability with heading angle χ (Kwon et al., 2019; Carette and van Walree, 2019), without consistent conclusions, or the influence of the wave period (Mauro and Vassalos, 2022a). Therefore, introducing the variability of wave period and heading in time-domain dynamic simulation is a substantial improvement to reach a more reliable survivability prediction, especially for new vessel designs in operational conditions.

The present paper proposes a novel method for evaluating the survivability of specific damage cases in a selected sea area, based on the following main enhancements to state-of-the-art survivability calculations:

1. Adoption of combined $H_s - T_z$ direct statistics for the sea areas of potential interest for passenger ships (as suggested by Mauro and Vassalos (2022a)).
2. Perform a sensitivity analysis on the number of repetitions needed to evaluate survivability in a predetermined sea area.
3. Perform a sensitivity analysis on the heading angle considering a fixed yaw angle ψ.

The sensitivity analysis on the repetitions is applied to a small sample cruise ship for two critical collision damages and two side grounding damages, performing the analyses in three different sea areas: the Caribbean Sea, the Western Mediterranean and the Baltic Sea. The heading variations have been applied to the collision cases only, providing a full 0–360 degrees prediction for the most critical damage.

The paper provides in Section 2 a review of the state-of-the-art principles and methodologies to evaluate survivability with static and dynamic approaches. Then, Section 3 outlines the new method based on the joint $H_s - T_z$ statistic, while the sensitivity analyses on repetitions and headings is described in Section 5 for the reference cases (presented in Section 4). The methodology uses statistics derived from wave measurements available in the literature (i.e., wave scatter diagrams (Hogben et al., 1986)) but also works with more accurate site-specific data, if available. The results show the diverse survivability levels of the same damages in different sea areas, stressing the importance of modelling the wave period and heading angle to obtain a more reliable site-specific survivability prediction for a passenger ship.

2. Passenger ship survivability

Survivability is associated with the probability of a ship capsizing or sinking when subjected to a potential feasible flooding scenario. Hence, the survivability analysis provides proper insight into the design parameters affecting ship stability in flooding conditions. The in-force regulations on damage stability (IMO, 2009, 2020) provide the fundamentals of damage stability assessment for passenger ships. The framework considers only collisions, assuming the ship has an open-to-sea breach on one side with consequent large-scale flooding. The Attained Survivability Index A is the probabilistic measure of survivability prescribed by the regulations, with the following formulation:

$$A = \sum_{i=1}^{N_d} w_i \sum_{j=1}^{N_c} p_{ij} s_{ij} \tag{1}$$

where N_d is the number of draughts used for the assessment, N_c is the number of relevant analysed damage cases, and $\mathbf{w} = \left(w_1, \cdots, w_{N_d} \right) \in \mathbb{R}^{N_d}$ is a vector of weights associated with the calculation draughts. The most significant variables in Eq. (1) are p_{ij} and s_{ij}, which identify the generic elements of two bidimensional vectors:

$$\mathbf{p} = \begin{bmatrix} p_{11} & \cdots & p_{1N_d} \\ \vdots & \ddots & \vdots \\ p_{N_c 1} & \cdots & p_{1N_d} \end{bmatrix} \in \mathbb{R}^{N_d \times N_c} \tag{2}$$

$$\mathbf{s} = \begin{bmatrix} s_{11} & \cdots & s_{1N_d} \\ \vdots & \ddots & \vdots \\ s_{N_c 1} & \cdots & s_{1N_d} \end{bmatrix} \in \mathbb{R}^{N_d \times N_c} \tag{3}$$

$\mathbf{p}$ elements are the so-called p-factors, describing the probability associated with each damage case after a collision event, thoroughly described by Vassalos et al. (2022a) and whose derivation depends on the method utilised to generate the damages, namely zonal (Pawlowski, 2004) or non-zonal (Bulian et al., 2016; Mauro and Vassalos, 2022b). $\mathbf{s}$ are the so-called s-factors, which can be interpreted as the conditional probability of survival after a flooding event due to the damage cases and draughts analysed. According to the definition provided by Eq. (1), index A represents a conditional averaged probability of survival or, considering the different draughts, a weighted average. In the case of SOLAS2009 regulations, the definition of three loading conditions is prescribed, with the additional assumption to discard the possibility of flooding spaces above a horizontal subdivision. The rules for passenger ships require the satisfaction of a deterministic criterion $A \geq 0.9R$, where R is the Required Subdivision Index derived from vessel dimensions and persons carried onboard, stating a threshold for safety at each draught.

This definition derived from SOLAS regulations suits the evaluation of survivability in calm water with static calculations. The employment of a more direct approach based on rigid body time-domain calculations needs a different definition of survivability, especially considering waves. The following sections describe the problem, elaborated in detail by Vassalos et al. (2022c).

2.1. Survivability with static approach

The assessment of survivability with a static approach implies the determination of s-factors through empirical formulations using parameters derivable from the static residual GZ curve for all the intermediate flooding stages and the final flooding stage of a damage case. Therefore, according to SOLAS (IMO, 2020), the s_{ij} (s-factors) contributing to the A-index in Eq. (1) are determined as follows:

$$s_{ij} = \min_{1 < k < N_{stage}} \left(s_{int_{ijk}}, s_{final_{ijk}} s_{M_{ijk}} \right) \tag{4}$$

where s_{int} indicates all the survivability factors for the N_{stage} intermediate stages of flooding, s_{final} is the survivability in the final equilibrium stage, and s_M is the survivability to additional external heeling moments in the final equilibrium stage. Regulations report the detailed formulations and the calculation process for the static s-factors which, in any case, respect the necessity to be defined in $[0, 1]$ to represent the probability of survival in a specific flooding event.

From the static analysis, three different cases for the s-factor are possible:

1. $s_{ij} = 0$: cases where the Ship has an insufficient residual stability margin or where it is assumed as statically capsized.
2. $0 < s_{ij} < 1$: cases with a reduced reserve of stability, possibly dangerous if further additional loads (e.g. waves) occurred.
3. $s_{ij} = 1$: cases with sufficient reserve of stability to be considered safe.

Then the resulting s-factors, combined with the p-factors, determine the A-index according to Eq. (1), to be compared with the required subdivision index R. However, A-index is not the only survivability metric for a passenger ship, as alternative parameters like the Potential Loss of Lives (PLL) or the GM margin are more impactful from an operator's perspective.

Besides, a static assessment could be handy to identify a global vision of the Ship's vulnerability. Vassalos et al. (2022b) highlight that such a static risk profile may identify areas where risk control options (RCOs) can be identified but these may be too approximate to figure out a realistic and comprehensive vision of the flooding process. It would then become necessary to increase the fidelity level of survivability assessment, opting for a dynamic approach.

2.2. Survivability with a dynamic approach

A dynamic approach changes the definition of survivability as it was meant to be for static calculations or, more precisely, adds the opportunity to consider a physics-based approach not described in static analyses. The principal additions to the static problem are the proper stochastic modelling of irregular waves environment and the dependence of survivability to the exposure time t_e. The last consideration is valid not only in the case of waves, as the dynamic assessment involves time-domain simulations. Thus, simulating a still water case, the flooding process may not end in the given simulation time (equivalent to the exposure time in waves).

However, considering a probabilistic framework and the possibility of describing a still water case as a case with significant wave height $H_s = 0$, the following definition describes the s-factors:

$$s_{ij} = p\left(H_{s_{ij}} \leq H_{s_{ij}}^*\right) = \int_0^\infty f\left(H_s\right) p_s\left(H_s\right) \mathrm{d}H_s \tag{5}$$

where $f\left(H_s\right)$ is the probability density function describing H_s for collisions, and $p_s\left(H_s\right)$ is the probability of surviving flooding for the given damage in the given sea state. H_s^* is a critical wave height, identifying the limiting survival condition for the damaged Ship in the specific damage case. Considering an infinite exposure time ($t_e = \infty$), then Eq. (5) can be simplified as follows:

$$s_{ij} = p\left(H_{s_{ij}} \leq H_{s_{ij}}^*\right) = \int_0^{H_s^*} f\left(H_s\right) \mathrm{d}H_s \tag{6}$$

The formulation (6) is valid as the function $p_s\left(H_s\right)$ ideally converges to a step function centred on H_s^*:

$$p_s\left(H_s\right) = \begin{cases} 1 & \text{if } H_s \leq H_s^* \\ 0 & \text{elsewehre} \end{cases} \tag{7}$$

However, achievable simulation time with time-domain damage stability codes is not infinite (Ruponen et al., 2022a) but ranges from a minimum of 30 minutes to 3 hours (Cichowicz et al., 2016). Hence Eq. (6) needs to be reworked, including the exposure time t_e. Such an inclusion leads to the following formulation:

$$s_{ij}|_{t=t_e} = \int_0^\infty f\left(H_s\right) p_s\left(H_s\right)|_{t=t_e} \mathrm{d}H_s \tag{8}$$

As the inclusion of the simulation time in Eq. (8) neglects the validity of the relationship (7), there is no longer a specific wave height H_s^* dividing the survivability space between capsize cases and safe cases. An interval of H_s is subject to the transition $0 < p_s(H_s) < 1$. Such a band, called *capsize band*, varies with the exposure time t_e (Tsakalakis et al., 2010) and vessel loading conditions (Spanos and Papanikolaou, 2012), namely draught and GM of the ship. Even though extremely simplified analytical formulations (based on Normal approximation or Sigmoid function)are present in the literature (Cichowicz et al., 2016), the most convenient way to determine $p_s(H_s)$ at each H_s is through the survival rate between multiple repetitions N_r, as it is arguable that the occurrence of an extreme event, as the capsize, follows a Normal distribution. Then, considering a fixed number of wave heights N_H, the dynamic survivability for a damage case becomes:

$$s_{ij}|_{t=t_e} = \sum_{h=1}^{N_H} p(H_{s_h}) \frac{1}{N_r} \sum_{k=1}^{N_r} I_{hk} \tag{9}$$

where $p(H_{s_h})$ is the probability associated to the hth H_s, $1/N_r \sum I_{hk}$ is the survival rate, and I_{hk} is an operator defined as:

$$I_{hk} = \begin{cases} 1 & \text{if the vessel survives after } t = t_e \\ 0 & \text{otherwise} \end{cases} \tag{10}$$

The last term that needs to be defined to evaluate the survivability with Eq. (9) is $p(H_s)$. The probability of a single wave height event is associated with the probability density function $f(H_s)$ used to model the wave occurrence. The praxis after project (HARDER, 2000-2003)
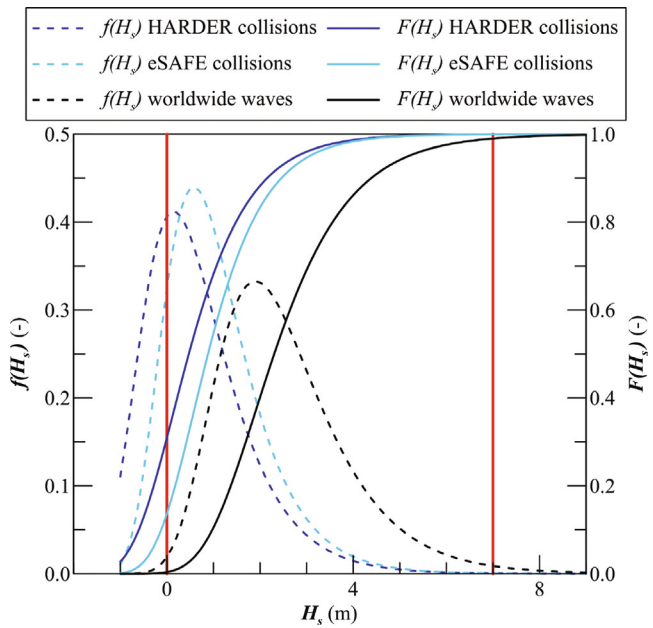

Fig. 1. Wave height distributions for damage stability calculations.

consists in using marginal cumulative distributions for H_s having the following general formulation:

$$F\left(H_s\right) = \exp\left(\exp\left(a - bH_s\right)\right) \tag{11}$$

which corresponds to the following probability density function:

$$f\left(H_s\right) = b \exp\left(a - bH_s - \exp\left(a - bH_s\right)\right) \tag{12}$$

Considering H_s from collision accident statistics, regression parameters were initially set to $a = 0.16$ and $b = 1.12$, leading to 99% of the sea states below $H_s = 4$ m. After successive reanalyses of accidents (Ventikos et al., 2018; eSAFE, 2017-2018), the problem's vision has changed towards a sea-state definition independent from accident occurrence. Foreseeing the constant evolution of passenger ships' operational profiles throughout worldwide operations, Luhmann et al. (2018) proposes new values for regression parameters ($a = 1.7171$, $b = 0.9042$) based on global wave statistics, imposing an upper truncation limit of 7 m to avoid unrealistically high H_s. Fig. 1 compares the provided H_s distributions, highlighting how the last worldwide regression proposal increases the probability of higher sea states compared to collision-based events. However, this modelling has a probabilistic weakness. Limiting the analyses between $0 \leq H_s \leq 7$ meters implies employing left and right-bounded distributions to preserve the definition of probability and effective applicability of Eq. (9). Such a matter is also in need of updating, even though the inversion process adopted to sample the H_s in a damage stability framework hides the problem with the truncation process.

To improve the analysis of operational conditions in the ship survivability assessment, modelling realistic environmental conditions is essential. Regardless of adopting a more correct truncated distribution, the approach using environmental modelling according to an equation similar to (11) is still an approximation, as it considers only H_s. It is, therefore, useful to study an alternative method to assess survivability after an accident in a realistic operational environment, which means an operational sea area.

3. Survivability in an operational sea area

The survivability evaluation in a specific operational area requires adopting some assumptions for modelling the sea environment, which

is generally associated with an irregular wave condition, characterised by a significant wave height H_s, a wave period (typically zero crossing T_z or peak T_p), and an encounter angle χ between the ship and the wave predominant direction. Besides, it is possible to refer to long-crested or short-crested scenarios, modelling the sea states with specific wave spectra that account for the aforementioned characteristics. However, a wave spectrum reflects only one combination of H_s and T_p for a given χ. For the survivability evaluation, it is then mandatory to identify the joint probability distributions $f(H_s, T_p, \chi)$ of H_s and T_p (or T_z) and χ for the operational area of interest.

Adopting a joint distribution implies a change in the formulation of dynamic survivability, as the traditional usage of $f(H_s)$ in Eq. (8) does not fit the new sea environment. The definition of dynamic survivability should be extended to higher dimensions in such a way to include the new modelling parameters, leading to the following formulation:

$$s_{ij}|_{t_e} = \int_0^{2\pi} \iint_0^\infty f\left(H_s, T_p, \chi\right) p_s\left(H_s, T_p, \chi\right)|_{t_e} dH_s dT_p d\chi \quad (13)$$

such definition is analogue to Eq. (8) but also considers the wave period and a generalised encounter angle between $(0, 2\pi)$. Furthermore, the probability of survival at the event $p_s(H_s, T_p, \chi)|_{t_e}$ is still representable with a capsize band. However, the band is not represented by a curve but by a hypersurface.

Direct application of Eq. (13) is problematic, as determining a joint distribution for wave and encounter conditions may be challenging to define. The encounter angle χ combines the vessel heading and wave environment; thus, it is not only an environmental characteristic but depends on the vessel's behaviour. It is, therefore, necessary to make some assumptions for the enhanced environmental modelling and consequent evaluation of survivability.

3.1. Proposed environmental modelling

As a first assumption, it is likely to consider the heading χ independent from the wave parameters. Then Eq. (13) can be rewritten as follows:

$$s_{ij}|_{t_e} = \int_0^{2\pi} f(\chi) \iint_0^\infty f\left(H_s, T_p\right) p_s\left(H_s, T_p, \chi\right)|_{t_e} dH_s dT_p d\chi \quad (14)$$

with $f(\chi)$ as the marginal distribution of headings and $f(H_s, T_p)$ as the joint distribution of wave heights and periods. Such modelling allows for considering waves separate from the heading, thus adopting distributions suitable for all incoming directions or specific for selected angles of occurrence. In the current approach to environmental modelling, the first option is selected, being more general and easier to represent with discrete (Hogben et al., 1986) or continuous (DNV, 2014) data available from the literature. Statistics of wave measurements can be found in the form of discrete scatter diagrams or by employing continuous distributions derived from specific probabilistic laws capable of approximating the joint $f(H_s, T_z)$, preferring T_z to T_p, as visualised in Fig. 2. Eq. (14) presumes the application of a continuous joint distribution for the wave environment, derived by combining two marginal distributions through copulas or by using one marginal for the first parameter and a conditional one for the other. Fig. 2(a) shows the second option, using a marginal two-parameters Weibull distribution for the H_s and a Log-normal model for the conditional T_z distribution. Fig. 2(b) provides the alternative discrete joint distribution typical of wave recording statistics, often the base for determining the continuous models as presented in Fig. 2(a).

Modelling irregular wave environments requires particular attention, regardless of the method used to approximate the joint wave distribution. Conventional hypotheses in damage stability, discussed in Section 2.2, consider identifying a significant wave height for a simulation. The associated wave period T_z derives from a simplistic assumption of considering a constant wave slope $\sigma = H/\lambda$ of 0.02, where λ is the wavelength. Then, the associated wave systems relate

only to specific combinations of H_s and T_z, not covering the entire sea area of interest, nor ensuring the coverage of most probable or extreme events. Furthermore, modelling the irregular wave system in damaged stability problems typically employs a general Pierson–Moskowitz (PM) spectrum (Pierson and Moskowitz, 1963) with the following two parameters form:

$$S_{\zeta PM}(\omega) = \frac{5}{16} H_s^2 \omega_p^4 \omega^{-5} \exp\left[-\frac{5}{4}\left(\frac{\omega}{\omega_p}\right)^{-4}\right] \quad (15)$$

or its extension to the following JONSWAP (J) model (Hasselmann and Olbers, 1973) with reported standard parameters:

$$S_{\zeta J}(\omega) = A(\gamma) S_{\zeta PM}(\omega) \gamma^{\exp\left[-\frac{1}{2}\left(\frac{\omega-\omega_p}{\sigma_J \omega_p}\right)^2\right]} \quad (16)$$

$$\sigma_J = \begin{cases} 0.07 & \text{if } \omega \leq \omega_p \\ 0.09 & \text{if } \omega > \omega_p \end{cases} \quad (17)$$

$$A(\gamma) = 1 - 0.287 \ln\gamma \quad (18)$$

$$\gamma = 3.3 \quad (19)$$

with γ the peak shape/enhancement parameter, σ_J a curve slope constant, ω the circular frequency and $\omega_p = 2pi/T_p$ the peak frequency of the spectra.

An alternative representation of the J-spectrum parameters enhances the irregular sea state environment modelling, including gamma variability across the possible combination of T_z and H_s. The J-spectral formulation is a suitable general model describing sea states ranging in $3.6 < T_p/\sqrt{H_s} < 5$ once more specific data are unavailable (DNV, 2014). The subsequent model allows for modelling γ as a function of T_p and H_s, according to the following equations set:

$$\gamma = \begin{cases} 5 & \text{if } \frac{T_p}{\sqrt{H_s}} \leq 3.6 \\ \exp\left(5.75 - 1.5\frac{T_p}{\sqrt{H_s}}\right) & \text{if } 3.6 < \frac{T_p}{\sqrt{H_s}} < 5 \\ 1 & \text{if } \frac{T_p}{\sqrt{H_s}} \geq 5 \end{cases} \quad (20)$$

As Eq. (16) and (20) consider T_p instead of T_z, it is necessary to identify a correlation between T_p, T_z and the γ parameter. A possible solution is as follows:

$$\frac{T_z}{T_p} = 0.6673 + 5.037 \cdot 10^{-2}\gamma - 6.23 \cdot 10^{-3}\gamma^2 + 3.341 \cdot 10^{-4}\gamma^3 \quad (21)$$

Eq. (21) relates T_p and T_z through a polynomial formulation of γ. However, being γ a conditional parameter to T_p, the resolution of the process requires an iterative calculation within the validity limits of γ. The validity range for the peak enhancement parameter is in $1 \leq \gamma \leq 7$, thus, Eq. (21) should be adequately limited to avoid inconsistencies in the iterative determination of gamma. However, the bounds provided by Eq. (20) are more restrictive than the existence domain of γ, ensuring validity for Eq. (21) through the possible couples of H_s and T_z of a sea area.

Fig. 3 shows the spectral density of the enhanced J-based environmental conditions compared with the standard PM and J spectra with constant H/λ ratio for three reference wave heights H_s: 1.5, 3.5 and 5.5 m, respectively. The extended capability of the new modelling is self-evident, and the figure allows for visualising the transition between PM-like spectra ($\gamma = 1$) and spectra with enhanced peaks ($\gamma > 1$) across different periods T_z for the same H_s. Nowadays, such modelling is widely adopted for seakeeping intact-ship analyses and could also apply to damaged stability problems. During Project FLARE, the model test design performed on a reference cruise ship made a step towards this environmental modelling (van Basten-Batemburg et al., 2020), resulting in test conditions employing a J-shaped spectrum with different γ values from 3.3. However, only a few participants in the benchmarking activities simulated the sea state with the tested spectral formulation, preferring the standard J with $\gamma = 3.3$ embedded in their codes (Ruponen et al., 2022b), and used for previous test cases on a
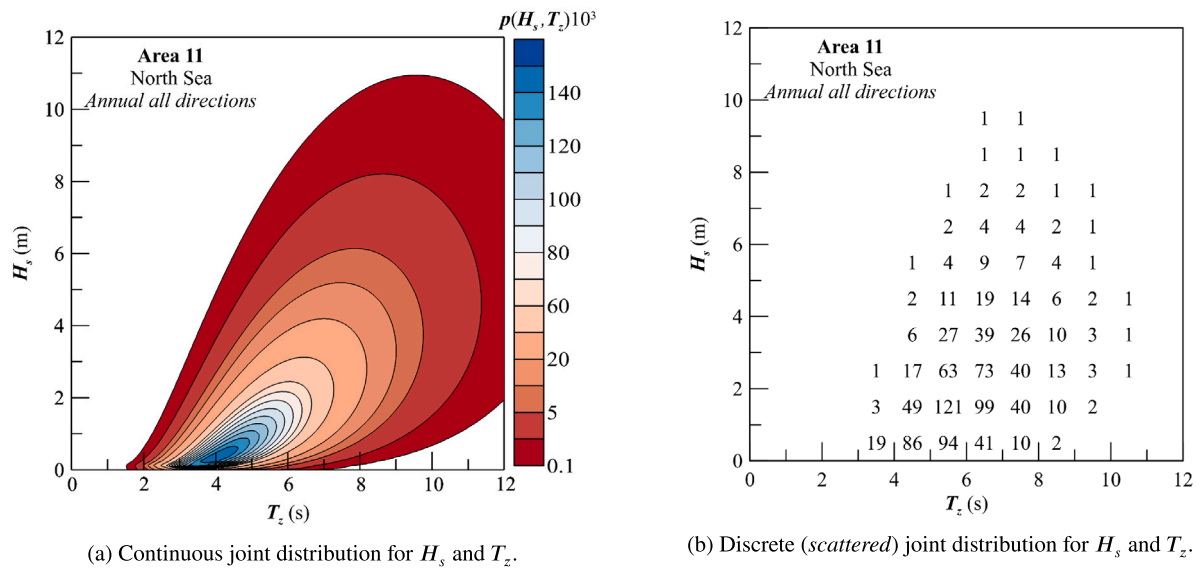
(a) Continuous joint distribution for H_s and T_z.

(b) Discrete (*scattered*) joint distribution for H_s and T_z.

Fig. 2. Different statistical representation for the reference sea Area 11 (North Sea).
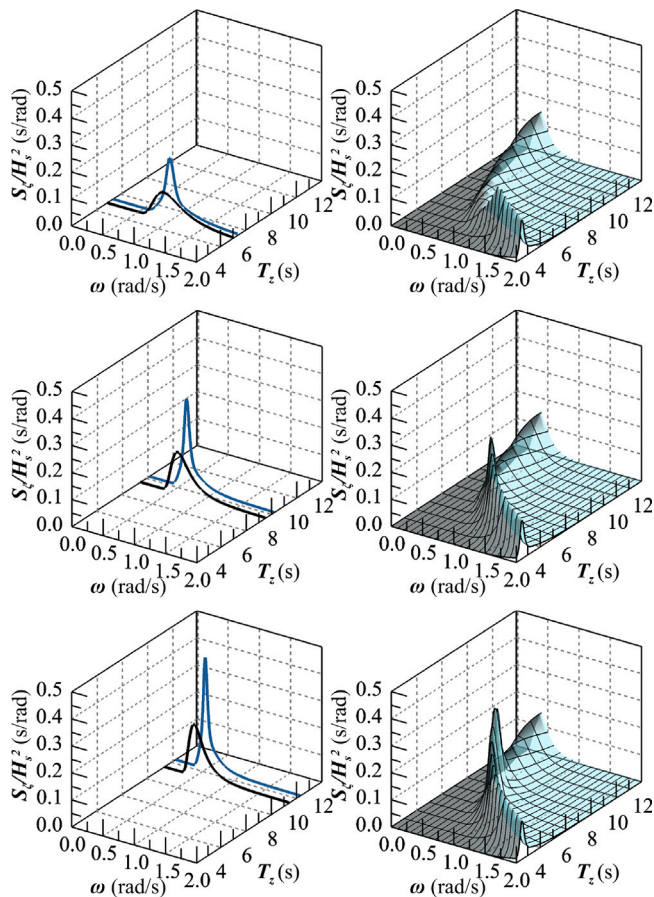

Fig. 3. Differences between conventional damage stability spectral densities (*left*) and enhanced ones (*right*) for $H_s = 1.0$ m (*top*), $H_s = 3.5$ m (*middle*) and $H_s = 5.5$ m (*bottom*).

Ropax (Ruponen et al., 2022a). According to the enhanced modelling, a J-shaped spectrum with $\gamma = 3.3$ does not represent a condition where H/λ value is 0.02. Such a condition corresponds to a $\gamma = 1$, thus to a PM spectrum.
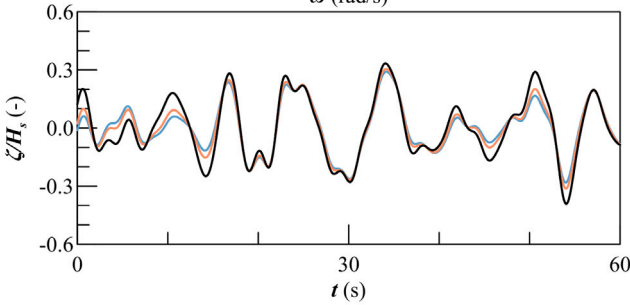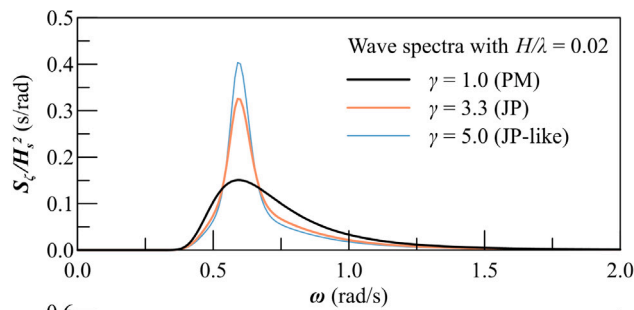
However, the spectral shape changes the generated wave-train in a time-domain simulation and, consequently, the wave-induced body forces acting on the vessel. Fig. 4 shows the magnitude of the spectrum shape change on the generated wave-train considering constant $H_s = 3.5$ m. The figure illustrates the two aforementioned different possibilities, thus, constant or variable H/λ. Figs. 4(a) and 4(b) maintain the same gamma values, and the wave-trains refer to the same phases (only amplitudes change between reported curves), neglecting from the representation the stochastic effect of irregular waves. Fig. 4(a) shows that the differences in γ for the conventional modelling with constant H/λ are changing just the amplitude of the individual oscillations, whilst Fig. 4(b) highlights more changes because of the different peak periods. It is, therefore, expected that considering wave period variations will change the loads more consistently than the variations between PM and JP spectra in the conventional damage stability assessment.

The above considerations are valid for a long-crested sea without the presence of a swell. However, such a model can be applied by superposing a swell and considering an additional directional spreading parameter for short-crested sea modelling.
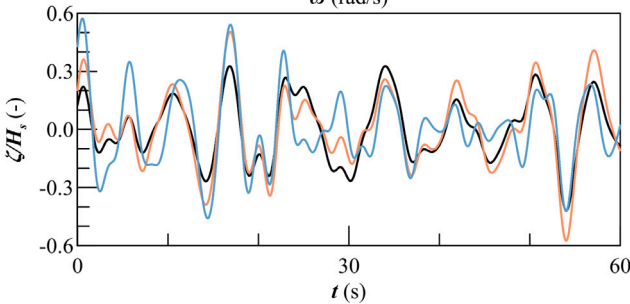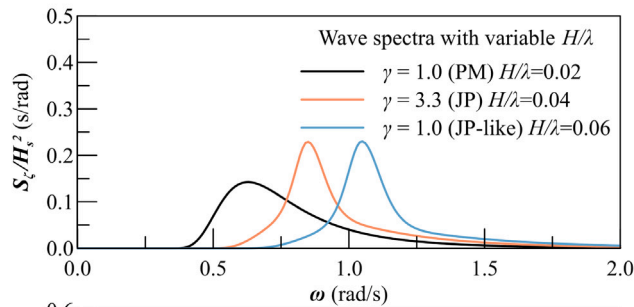
3.2. Survivability of a damage scenario

The last alternative for calculating survivability in an operational sea area is selecting a continuous or a discrete model for the joint distribution of wave parameters $f(H_s, T_z)$. For the present work, the discrete option is the most suitable for preliminary study, requiring fewer calculations than a continuous approach.

Having determined the spectral formulations for the environmental settings, it is then possible to perform the dynamic simulations for the specific cells of a scatter diagram according to the granularity of the provided statistics for H_s and T_z. For example, the widely diffused discretisation employed by the Global Wave Statistics (Hogben et al., 1986) implies simulating H_s in steps of 1 metre and T_z in steps of 1 second, limiting the environmental conditions to the cells containing observed data. Taking Area 11, shown in Fig. 2(b), as a reference, a number $N_{cl} = 53$ of cells is present. Therefore, recalling Eq. (9) for a fixed number of simulations, the total amount of calculations for a damage case is $N_{tot} = N_{cl} N_r$, with N_r the number of repetitions on a single cell to consider the stochastic nature of irregular waves. A continuous approach to sea area modelling necessitates sampling couples (H_s, T_z) from the joint distribution, therefore using a much higher number of simulations employing Monte Carlo or Quasi-Monte Carlo-like methods as it is the case for the damage breach generation.

s_A formulation and facilitate the graphical representation of quantities, leading to the following equation:

$$s_A = \sum_{i=1}^{N_\chi} p(\chi_i) \sum_{k=1}^{N_H} \sum_{h=1}^{N_T} p(H_{s_k}, T_{z_h}) s_{ikh} \quad (23)$$

or, considering the survivability for a single angle χ:

$$s_{A_\chi} = \sum_{k=1}^{N_H} \sum_{h=1}^{N_T} p(H_{s_k}, T_{z_h}) s_{kh} \quad (24)$$

The resulting calculation framework is then similar to operability calculations used for ship motions (Gutsch et al., 2020) and successfully extended to other fields of hydrodynamics as dynamic positioning in discrete (Mauro and Prpić-Oršić, 2020) and continuous form (Mauro and Nabergoj, 2022), encouraging its application to ship survivability.

However, it is necessary to figure out the initial conditions to set up the survivability assessment of a critical case with dynamic simulations. Experience gained with the recent international benchmark activities on damage stability (Ruponen et al., 2022a,b) highlights that the initial settings for complex rigid-body time-domain simulations are strictly related to the code employed to perform the calculations. For the initial development of the scatter diagram methodology for damage stability assessment, Mauro and Vassalos (2022a) provided the following settings and assumptions:

- *Simulation type*: rigid-body time domain simulation in 4 degrees of freedom (sway, heave, roll and pitch motions), including coupling with internal water motions. Water ingress/egress modelled with the Bernoulli equation.
- *Body forces*: Froude–Krylov components integrated on the actual wetted surface and first-order wave forces evaluated by 2D strip theory calculations at different ship attitudes. Drift forces modelled with empirical models.
- *Initial conditions*: the vessel is initially intact with a fixed heading of 90 or 270 degrees (according to the Damage side).
- *Environmental conditions*: H_s and T_z are according to the granularity of a Global Wave Statistics scatter diagram. Waves are modelled with a JONSWAP spectrum with variable γ. No additional current and wind loads.
- *Simulation time and repetitions*: a time t_e of 30 minutes (Vassalos and Paterson, 2022) applies to all the tested environmental conditions. Each simulation is repeated for 10 times (Spanos and Papanikolaou, 2014; Cichowicz et al., 2016), to take into account the effect of random phases in the wave realisations.

The above settings are presenting the state-of-the-art for damage stability calculations in irregular waves by means of rigid-body time domain simulations, except for the new proposed environmental modelling. The assumptions reflect, especially concerning the simulation time t_e a compromise solution between accuracy in detecting critical damage conditions and calculation time needed to perform the damage stability assessment. Fig. 5 shows an example of the scatter-diagram approach on a notional case according to the above settings. The representation refers to Area 11 (the North sea) on an arbitrary damaged ship on the starboard side, showing the behaviour of the capsizes ratio s_{hk} across the scatter cells. The case is purely indicative as the higher wave heights are also above the validity limits of the codes used for the simulations. The four scopes on time series (*a*, *b*, *c* and *d*) at the reference $H_s = 3.5$ m show the process of determining s_{hk} from the time traces of the roll motion ϕ (the most significant to visualise a capsize case). From the figure, the effect of the period change is evident. In the reported case, based on $N_r = 10$ repetitions, a change of 4 seconds in the period (from 7.5 seconds of case *a* to 10.5 of case *d*) led to transitioning from zero to more than 50% capsize cases. Therefore, the approach is relevant to an enhanced damage stability assessment, and more detailed analyses can supersede the initial assumptions reported above.

(a) Conventional damage stability modelling with constant H/λ.

(b) Enhanced modelling with variable H/λ.

Fig. 4. Wave realisations with different amplitude spectra and same phase for $H_s = 3.5$ m.

The selection of the scatter diagram approach necessitates a discrete formulation of Eq. (14). The survivability $s_{ij}|_{t_e}$ will be renamed s_A to simplify the indices and the time dependency nomenclature, referring to a single damage scenario intrinsically associated at an exposure time t_e. Then, reusing arbitrary indices, Eq. (14) is discretised as follows:

$$s_A = \sum_{i=1}^{N_\chi} p(\chi_i) \sum_{k=1}^{N_H} \sum_{h=1}^{N_T} p(H_{s_k}, T_{z_h}) \frac{1}{N_r} \sum_{j=1}^{N_r} I_{ijkh} \quad (22)$$

where $p(\chi_i)$ is the probability associated with the ith heading angle, $p(H_s, T_z)$ is the probability associated with the hth H_s and kth T_z, and $1/N_r \sum I_{ijkh}$ is the survival rate with I_{ijkh} defined according to Eq. (10). Eq. (22) intrinsically implies the utilisation of an omnidirectional scatter diagram, as the wave joint probability is not associated with the encounter angle. Rewriting the survival rate is advisable to simplify
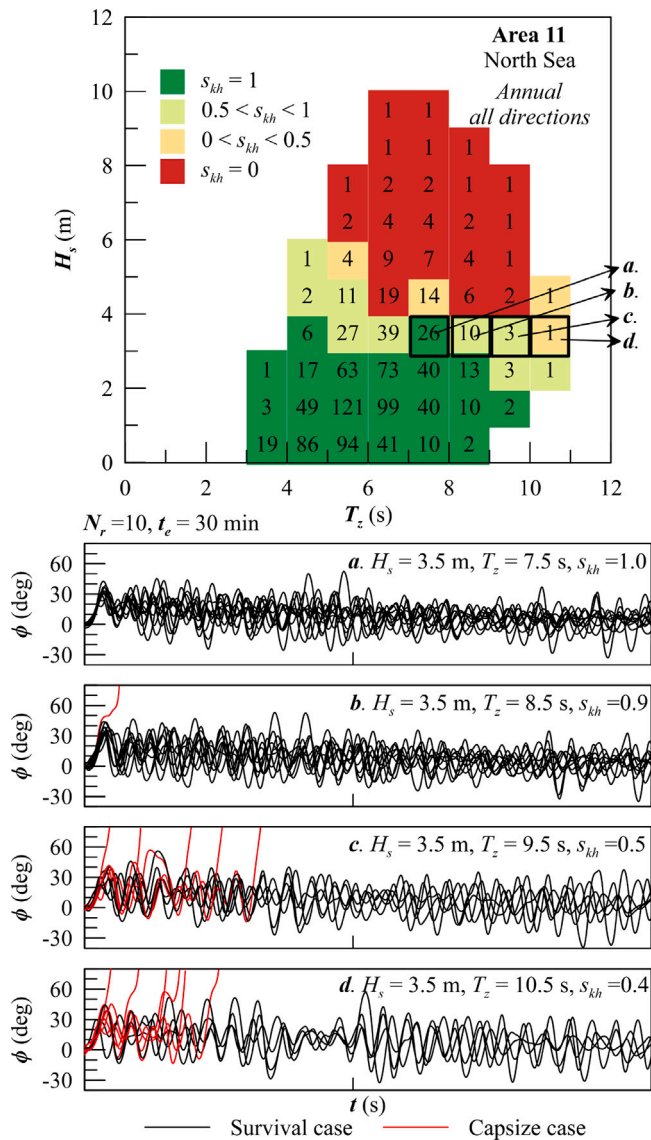
Fig. 5. Notional example of the survivability $s_{A,hi}$ of a damage scenario for a single heading $\chi = 90$ deg on a scatter diagram.

Table 1
Main characteristics of the reference ship.

Parameter	Symbol	Value	Unit
Length over all	L_{OA}	128.0	m
Length between perpendiculars	L_{PP}	113.7	m
Subdivision length	L_s	125.8	m
Breadth	B	20.0	m
Calculation draught	T	5.1	m
Calc. vertical centre of gravity	KG	9.584	m
Number of passenger	N_{Pass}	323	–
Number of crew	N_{crew}	155	–
Deadweight	DWT	1250	t
Calculation displacement	Δ	8404	t
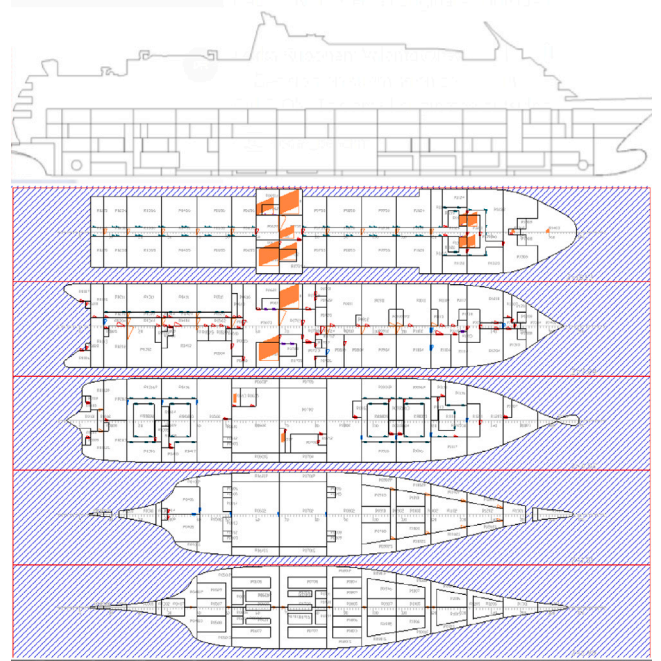
Fig. 6. Reference ship lateral profile and general arrangement used for dynamic calculations.

4. Reference case

The capabilities extension of the scatter diagram approach beyond the standard initial conditions reported in the preliminary study requires additional analyses. To this end, it is necessary to identify a proper set of reference cases in compliance with the initial investigation.

First of all, the same reference ship has been chosen, considering the same loading conditions of the preliminary study and relevant damage cases. The same is for the reference areas, opting for the sites of interest for passenger ships and where environmental conditions remain within the limits of the codes used for damage stability assessment. The following sections give a more detailed overview of the ship, the damage cases and the reference areas.

4.1. The reference ship

The present study employs one of the sample ships (Luhmann, 2019) available within the (FLARE, 2018-2022) project, already used in the preliminary investigation (Mauro and Vassalos, 2022a). This specific vessel is a small cruise ship with a total capacity of 478 people on board. Table 1 lists the main characteristics of the cruise ship, and Fig. 6 shows an overview of the vessel's profile and internal layout. The ship complies with SOLAS 2020 probabilistic damage stability and has been modelled considering 271 compartments and 227 internal openings, which is a suitable granularity for dynamic simulations (Guarin et al., 2021).

As the ship has a subdivision length L_s below 198 m, the maximum damage length for collisions will be $10/33L_s$ with a significant higher $L_x/L_{x,max}$ ratio compared to longer ships (Mauro et al., 2022b), with L_x being the damage longitudinal length and $L_{x,max}$ the maximum damage longitudinal length, respectively. Therefore the vessel is a suitable candidate to identify critical damage cases compared to other larger passenger ships present in the initial set of FLARE sample ships, as already highlighted in previous studies (Guarin et al., 2021).

However, this study addresses also side groundings. The probabilistic models for collisions and side groundings admit two different values for the $L_{x,max}$ on the reference ship; the collision damages, as mentioned above, allow for $10/33L_s$, and side groundings extend the limit to $0.632L_s$ resulting in 38.12 and 79.51 m, respectively. Such a matter influences the following representation of critical cases in non-dimensional form.

4.2. The reference damage scenarios

The preliminary study on the scatter diagram approach employs a set of 4 reference damages: two collisions and two side-grounding cases. Damage cases refer to survivability analyses performed with static calculations on an initial set of 30,000 breaches, equally distributed between damage types. Breach definition employed damage dimensions/locations distributions specific for collisions, side and bottom grounding damages following a non-zonal approach (Bulian et al., 2020; Mauro and Vassalos, 2022b). Conventionally in the static procedure, the breaches involving the same compartments constitute the so-called damage cases, statically analysed without considering differences in the hull breach dimensions.

A damage case is a problem-simplification transitioning to dynamics, as it misses the information on the breach dimension, which is essential to simulate the inflow/outflow rate. Therefore, to reconsider the breach dimension, the damage representative of the higher lateral projected area has been considered, as a first assumption, the representative breach for dynamic calculations on a damage case. Calculations have been performed on a restricted set of damage cases. As described by Mauro et al. (2023), a preliminary subset of critical damages has been filtered considering the static calculation results, retaining only damage cases with a factor $p(1 - s)$ above an arbitrary threshold of $2 \cdot 10^{-4}$. The analysis of the filtered cases continues with dynamic simulations, performing calm water calculations with $t_e = 3$ hours aimed to identify potentially critical damages worthy of investigation in irregular waves employing specific dynamic survivability criteria (Mauro et al., 2022b). Such criteria aim to identify cases not leading to a true capsize but potentially dangerous in case additional loads occur. The criteria are (Guarin et al., 2021):

A. *SOLAS heeling*: final average heel above ±15 degrees.
B. *ITTC maximum heeling*: maximum heeling above ±30 degrees.
C. *ITTC average roll*: cases where 3 minutes' average roll exceeds ±20 degrees.
D. *Large floodwater mass rate*: cases where the mass rate is above 2000 t/h at t_e.

It has to be noted that criterion D has been established for large passenger ships; therefore, it can be reasonable to adopt a lower threshold value for smaller cruise vessels as the reference ship. However, during project FLARE, the same threshold has been used for large and small passenger ships during the damage stability assessment (Guarin et al., 2021). Furthermore, the criterion has been found as less critical than others, regardless of the vessel size. For such a reason, the threshold value for criterion D is kept at 2000 t/h, even though a displacement-dependent threshold could be worthy of investigation in future research projects.

Besides dynamic criteria, the categorisation of actual capsizes could be an interesting output of preliminary dynamic analyses (Mauro et al., 2022a), distinguishing between events occurring during the first oscillations of the damaged ship (the so-called *transient* cases) or afterwards when the flooding process is ongoing or finished (*progressive* or *stationary-state* capsizes).

The results for the reference ships highlight 90 'true' capsizes for collisions and 72 for side groundings, including 64 and 67 transient cases. Besides, 113 collision scenarios and 107 side groundings fail at least one of the dynamic criteria without leading to a capsize in the simulated time, being potential critical cases leading to a capsize in an irregular sea environment. The remaining scenarios could be considered safe, as a first approximation, in case of adverse weather. Table 2 provides an overview of the screening of the preliminary dynamic simulations results, showing also the damage cases failing each of the possible combinations between dynamic criteria A, B, C and D.

Besides the tabular representation, Fig. 7 gives a graphical representation of the damage cases' longitudinal location and length in

Table 2
Final status of preliminary dynamic simulation and dynamic criteria failed by critical cases.

	Final status	Collision	Side grounding		
	Safe	20	85		
	Capsize	26	5		
	Transient capsize	64	67		

Criteria	Collision	Side gr.	Criteria	Collision	Side gr.
A	48	51	B,C	0	0
B	0	0	B,D	0	0
C	0	0	C,D	0	0
D	2	9	A,B,C	13	8
A,B	16	22	A,B,D	4	3
A,C	20	9	B,C,D	0	0
A,D	4	2	A,B,C,D	0	1

non-dimensional form, providing the categorisation between capsizes (including transient cases), failing criteria instances and safe conditions. it is interesting to notice that for the collision cases, two critical areas appear: one in the aft and one in the fore shoulder of the ship (see Fig. 7(a)). For the side groundings in Fig. 7(b), the critical area corresponds to the fore shoulder only without presenting a concentration of criticalities in the aft end of the ship. Such behaviour is mainly due to the marginal distributions of the damage locations, which differs between collisions and side groundings. Collisions are uniformly distributed across the subdivision length while side groundings present a higher density in the fore ship (Bulian et al., 2020), thus resulting in different areas for criticalities.

Simulations leading to capsize already in a calm water environment are not of interest for irregular wave simulations as they almost lead to 100% capsizes adding external wave loads. On the other hand, safe cases are not particularly interesting as they may be subject to capsizing conditions with considerable high H_s, thus for conditions not appropriately modelled by dynamic simulation codes. Therefore, the selection of critical scenarios pertains to cases where the simulation does not satisfy the above-mentioned dynamic criteria (the light yellow dots in Fig. 7). The damage cases categorisation, reported in Table 2, highlights that few damages fail three criteria, whilst only one collision case falls all four dynamic criteria while surviving the simulation after t_e. Then, it is appropriate to focus attention to breaches that lead to a failure of one or at most two dynamic thresholds, representing the highest occurrence for both damage types.

Such damages have different locations and dimensions, inheriting the respective occurrences from the static p-factor analysis, which is a function of the internal layout and the probabilistic damage model. Therefore, cases with large longitudinal extensions are less probable than shorter ones for both the considered damage types. The preference is then for damages of medium longitudinal extension (between 10 and 30 m) but still capable of having a significant impact on the final ship attitude at the end of the flooding process, thus considering an added displacement due to water ingress of more than 15% of the intact one. Concerning the location, the choice goes for the most vulnerable areas detected in Fig. 7, thus the fore and the aft shoulder for collisions. The same selection also pertains to side groundings to cover comparable internal spaces of the ship, even though the area of the critical grounding is denser in the fore-ship. Besides, aiming for running dynamic simulation in waves with $t_e = 30$ minutes, the cases should reach a steady state of flooding before the 30 minutes in calm water.

Applying these criteria allows for selecting four cases: two collisions and two side groundings. Table 3 gives the main breach characteristics and the dynamic criteria failed by the considered criticalities. A brief description of the four damages, all located on starboard, is as follows:

DAM-1 is a collision case between the aft shoulder and midship. The damage in calm water fails only criterion A, reaching a maximum heeling of −26 degrees in the initial stage of flooding and
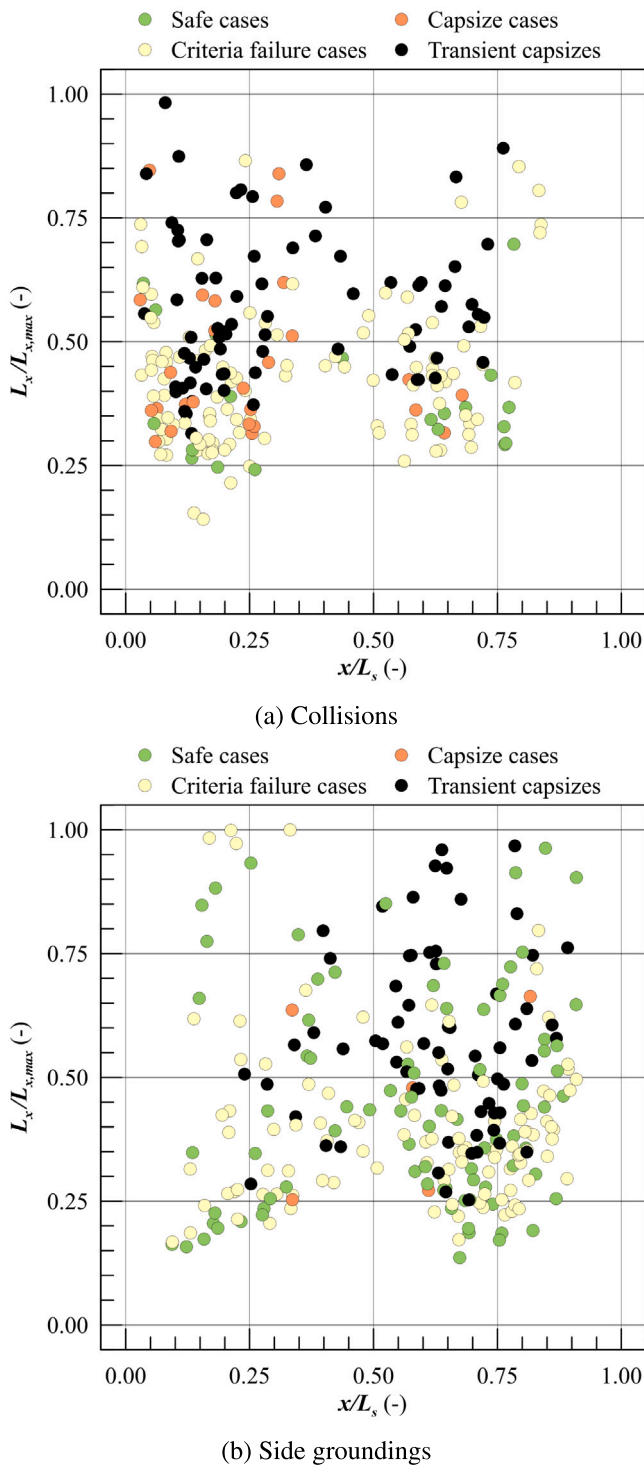
(a) Collisions

(b) Side groundings

Fig. 7. Damage categorisation of collision (a) and side groundings (b).
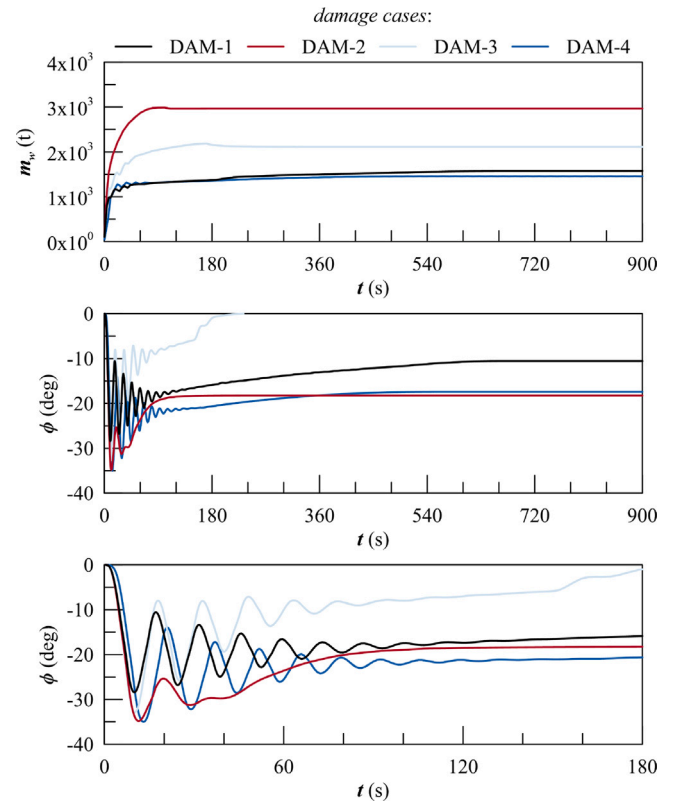

Fig. 8. Floodwater mass (*top*), ϕ angle time history (*middle*) and highlight on transient stage *bottom* in calm water for the four sample damages.

Table 3
Main characteristics of the reference damage cases for survivability analysis.

| Dam. ID	Dam. type	x_D	L_x	L_y	L_z	Criteria
DAM-1	collision	35.45	20.51	1.94	4.19	A
DAM-2	collision	64.29	12.05	6.83	8.71	A,B
DAM-3	side grounding	82.05	21.82	0.24	4.87	B
DAM-4	side grounding	51.13	25.82	0.57	2.96	A,B

then reaching a steady angle of about −15 degrees, as reported in Fig. 8, together with the amount of floodwater entered during the flooding process.

DAM-2 is a collision case across midship, with a lower length but higher penetration and height compared to DAM-1. The damage in calm water fails criteria A and B, reaching an initial heeling of about −35 degrees in the transient stage and a steady angle of −19 degrees, as reported in Fig. 8. The Figure shows that the amount of floodwater is almost three times that of DAM-1. The higher steady angle may indicate a more severe condition for simulations in irregular waves compared to DAM-1.

DAM-3 is a side grounding case between the midship and the fore shoulder. The damage in calm water fails only criterium B, reaching a maximum heeling above −30 degrees. After the transient stage, the flooding progress continues until the ship reaches almost even keel condition (see Fig. 8). The amount of floodwater is nearly double that of DAM-1.

DAM-4 is a side grounding case between the aft shoulder and midship. The damage in calm water fails criteria A and B, reaching a maximum heeling above −30 degrees and a final equilibrium heel below −20 degrees (see Fig. 8). The amount of floodwater is comparable to DAM-1.

Damages DAM-2 and DAM-4 reach a final equilibrium stage below an absolute value of 20 degrees for the heel angle. Hence, they do not fail criterion C, but they could still be even more dangerous than the other 2-failing criteria damages for irregular wave simulations. Fig. 9 shows the damage location and length of simulations failing
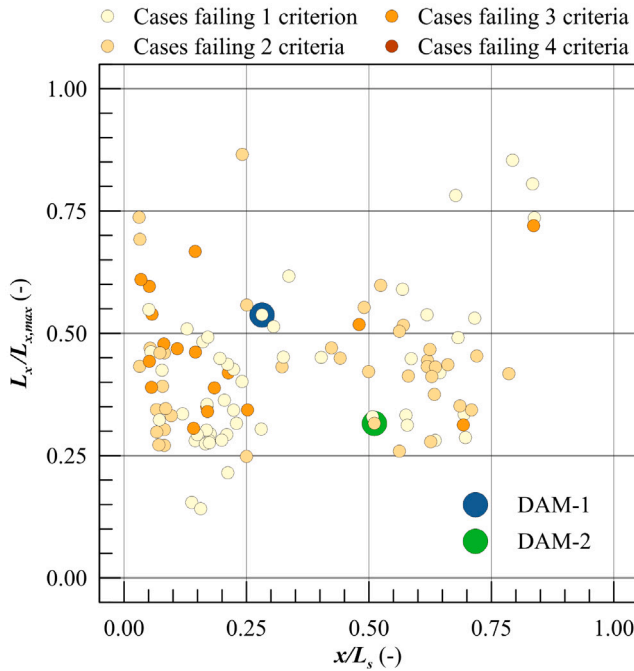
(a) Collisions
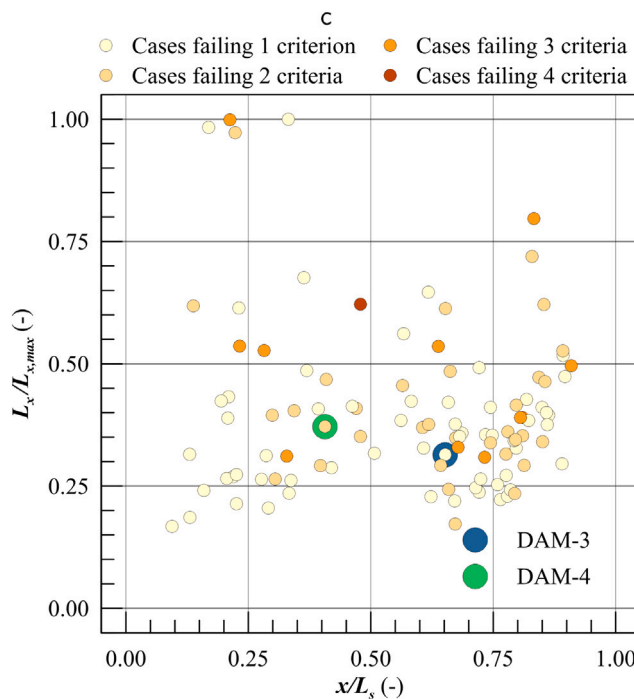
(b) Side groundings

Fig. 9. Non-dimensional location, length and number of failing criteria of the initial damage set of collisions (a) and side groundings (b).

the dynamic criteria for collisions and groundings, highlighting the number of thresholds exceeded by each simulation. Fig. 10 displays the longitudinal positioning of the already described critical damages selected for the subsequent analyses on survivability in an operational sea area.
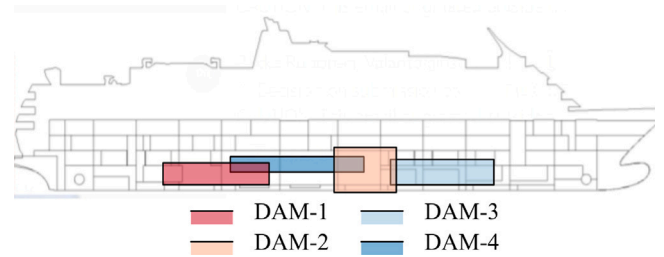

Fig. 10. Longitudinal location and dimensions of the for damages along the ship's profile.

4.3. Reference operational sea areas

With the test vessel being a small cruise ship, it is worth selecting as reference sea areas for the critical collision analysis of sea areas of the world that are of primary interest for cruises. The following sea areas are idoneous to have a more general environment suitable and significant for a large set of cruise ships: the Caribbean Sea (Area 47 for the Global Wave Statistics), the Western Mediterranean (Area 26) and the Baltic Sea (Area 5). Such a choice allows for avoiding extreme and particular operational areas that can be operated by dedicated ships only (e.g. Artic or Antarctic areas).

Fig. 11 shows the scatter diagrams of the three mentioned areas. It is possible to observe the different natures of the three sea areas; Area 47 presents waves not exceeding H_s of 6 m, but the wave periods could be up to 12 seconds, with higher density in the range between 6 and 8 seconds. Area 5 has the same limits for H_s, but the wave periods T_z are quite different, with higher density between 4 and 6 seconds and not exceeding 10 seconds. Area 26 has H_s limits up to 8 m, but the periods' limitations are comparable to Area 5.

The scatter diagrams are representative of an average statistics of a developed wide fetch sea area. However, the study considers also side groundings/contacts cases (i.e. DAM-3 and DAM-4) which most likely occur near shore or near harbours, where the environmental conditions may present lower values of H_s and in presence of relatively shallow waters. As such additional data are not available for specific cases, general scatter diagrams are applied also to the grounding case to demonstrate the approach on a different damage type than pure collisions.

5. Influence of operational area on ship survivability

The present Section reports the survivability analysis performed on the reference ship for the three reference sea Areas and four selected damages (all described in Section 4) according to the scatter diagram approach described in Section 3. The presentation of the results consists of two parts:

1. *Sensitivity analysis on N_r*: presentation of a set of simulations aiming at identifying a suitable convergence threshold for the survivability evaluation with a scatter diagram approach.
2. *Heading variations*: presentation of a set of simulations showing the effect of heading on survivability, considering yaw motion fixed.

All the reported data derive from time-domain simulations performed with code PROTEUS3 (Jasionowski, 2001), which solves the 6DOF rigid-body ship motion equations coupled with the floodwater dynamics. In this study, as usual for damage stability problems, ship dynamics is in 4DOF, neglecting surge and yaw motions. The flooding process is governed by Bernoulli's equation, while a lumped mass model describes the motion of water inside compartments. Froude–Krylov and restoring forces consider the instantaneous wave elevation
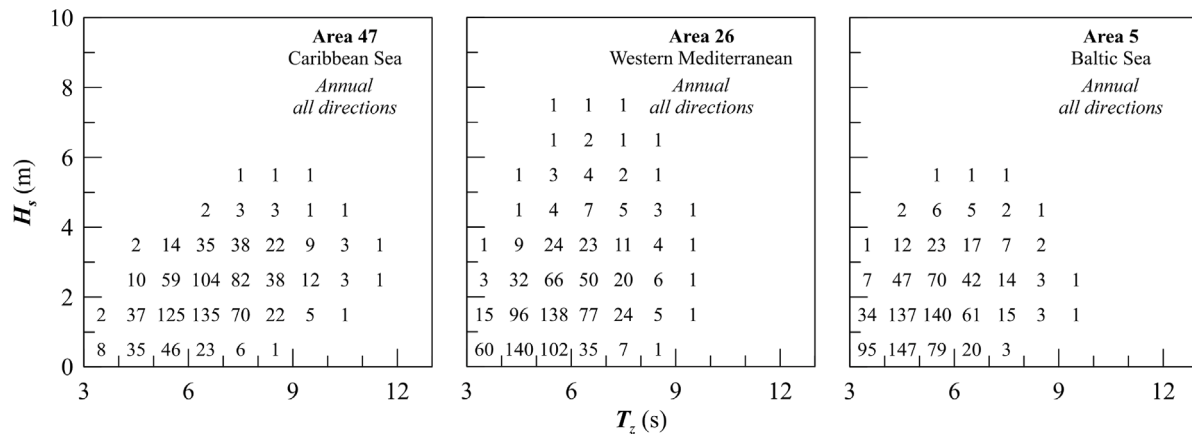
Fig. 11. Wave scatter diagrams of the principal sea areas of interest for passenger ships (Mauro and Vassalos, 2022a).

for regular and irregular waves, radiation and diffraction derive from 2D strip theory. Hydrodynamic coefficients vary with the vessel attitude during the flooding process. The vessel is assumed free to drift, with drift forces evaluated by empirical formulations. Here the indications are provided by trying to be more general as possible, giving more specific advice, where needed, only for the PROTEUS3 software used for the reported simulations.

5.1. Sensitivity on the number of repetitions

The preliminary study performed with a scatter diagram approach took into account a fixed number of repetitions $N_r = 10$. Here, N_r has been increased to 50 to analyse the variation of s_{A_χ} across the repetitions s for $\chi = 90$ degrees. Figs. 12 to 15 show the scatter diagram results on the three see areas at the fixed N_r of 10, 25 and 50 for DAM-1, DAM-2, DAM-3 and DAM-4, respectively.

Considering the collision damages, Fig. 12(a) shows the survivability in the three areas for DAM-1 with $N_r = 10$, Fig. 12(b) with $N_r = 25$ and Fig. 12(c) with $N_r = 50$. The differences in wave occurrences between the three scatter diagrams impact the s_{A_χ} value among the sea Area; however, the repetitions influence the result too. The colour change in the scatter cells visually highlights the differences, which lead to different survivability values. Analysing the reported s_{A_χ} variations with N_r area by area, it is evident that DAM-1 survivability is affected by environmental conditions with a H_s above 4 m, thus conditions with low occurrence in all the three sea Areas, especially for Area 5. Therefore, the survivability changes with N_r are small, below 1.5% (Area 47) or about 0.4% in the case of Area 5.

Fig. 13 shows the results for DAM-2 with $N_r = 10$ (Fig. 13(a)), $N_r = 25$ (Fig. 13(b)) and $N_r = 50$ (Fig. 13(c)). The damage case is more severe than DAM-1, leading to a lower survivability level in all three analysed sea Areas. The survival rate changes in the single cells modify the shape of the capsize region, which for DAM-2 extends in an area where wave occurrences are higher than for DAM-1. Consequently, the variability of the results obtained varying N_r is higher than in the previous case in all three sea Areas, reaching about 2.5% for Area 47 and being above 1% also for Area 5.

Switching to the side grounding cases, Fig. 14 shows the results for DAM-3 with $N_r = 10$ (Fig. 14(a)), $N_r = 25$ (Fig. 14(b)) and $N_r = 50$ (Fig. 14(c)). DAM-3 is the less severe of the four analysed damages, and for the three selected sea Areas, only one cell with survival rate equal to zero is present. Therefore, the variations of s_{A_χ} pertain only to the bi-dimensional *capsize band*, leading to little survivability level variations with N_r, all with a magnitude below 1%. Even though the differences are minor across the repetitions, the survivability value changes with the reference sea Area in line with variations observed for DAM-1.

At least, Fig. 15 shows the results for DAM-4 with $N_r = 10$ (Fig. 15(a)), $N_r = 25$ (Fig. 15(b)) and $N_r = 50$ (Fig. 15(c)). Even though

Table 4
s_{A_χ} values at different N_r for the four analysed damage cases in the three reference sea areas.

Dam. ID	N_r	Area 47	Area 26	Area 5
DAM-1	10	0.9593	0.9518	0.9769
	25	0.9495	0.9497	0.9756
	50	0.9444	0.9479	0.9745
DAM-2	10	0.7151	0.8507	0.8919
	25	0.7240	0.8489	0.8902
	50	0.7332	0.8594	0.9009
DAM-3	10	0.9498	0.9715	0.9863
	20	0.9680	0.9740	0.9884
	50	0.9673	0.9734	0.9886
DAM-4	10	0.7226	0.8680	0.9118
	20	0.7231	0.8708	0.9149
	50	0.7262	0.8665	0.9100

DAM-4 is a side grounding, it presents a survivability level similar to the collision case DAM-2. Therefore, the considerations valid for DAM-2 remain the same for DAM-4, with survivability variations between 2.5% for Area 47 and 1% for Area 5. As a final recap, Table 4 reports the survivability values at fixed N_r for all analysed damages and sea Areas.

A simple comparison of s_{A_χ} at the three N_r values reported in the graphic examples cannot establish the N_r value, which ensures the convergence of the survivability calculation. The process convergence can be checked by monitoring the relative differences between consecutive s_{A_χ} values:

$$\Delta s_{A_{\chi j}} = \left| s_{A_{\chi j}} - s_{A_{\chi j-1}} \right| \quad \text{for } j = 2, \cdots, N_r \tag{25}$$

where s_{A_χ} derives from Eq. (24).

The identification of adequate convergence thresholds is necessary to avoid the necessity of executing too many simulations to reach a reliable result. To this end, it is essential to understand the meaning of the variable under analysis and its relation to end-users necessities. The description of survivability with a scatter diagram approach introduces the concept of a downtime period, means the amount of time the vessel could survive in one year, parallel to the probability of capsizing in a given sea state. The adopted scatter diagrams have an annual definition, which means that survivability is associated with a fraction of a year where the ship can be considered safe in a sea Area after a given accident. It is then possible to quantify the threshold in terms of days a year, which means adopting a consolidated practice for vessel operability evaluation for onboard workability or Dynamic Positioning. Therefore, a convergence threshold of 1 day a year corresponds to a Δs_{A_χ} of $2.74 \cdot 10^{-3}$. Increasing the tolerable days a year increases the threshold value; like one of 5 days a year corresponds to a Δs_{A_χ} of
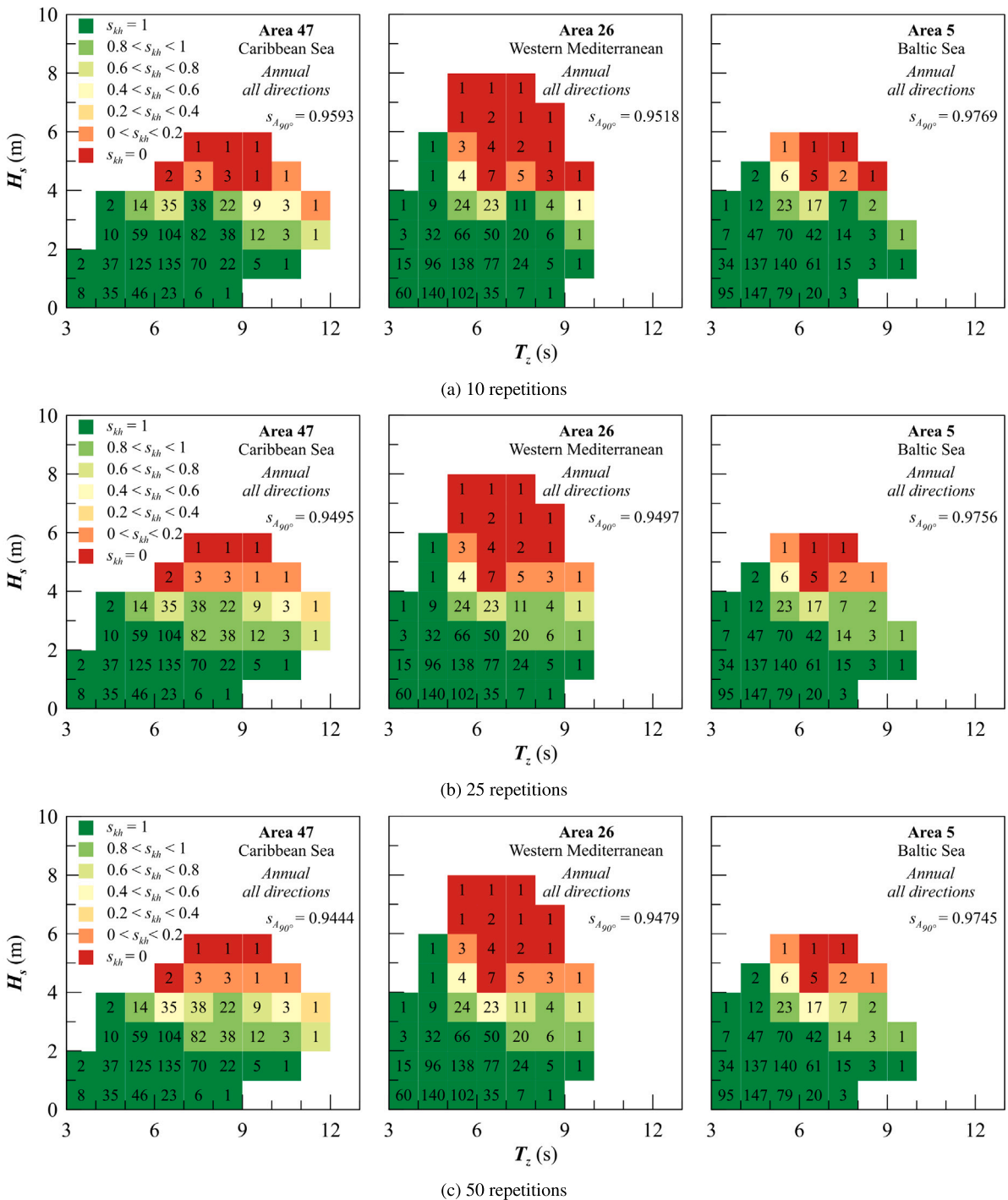
Fig. 12. DAM-1 survivability in the three selected sea areas considering 10 (a), 25 (b) and 50 (c) repetitions.

$13.70 \cdot 10^{-3}$, 30 days corresponds to $82.19 \cdot 10^{-3}$ and so on for all relevant thresholds.

Fig. 16 reports the variations of survivability s_{A_χ} and Δs_{A_χ} with N_r for the four analysed damage cases in the three reference sea Areas. For each sea Area, the upper graphs report the curves referring to the four damages, highlighting the differences in the survivability value of each damage across the three Areas. As also emphasised in Table 4, the differences are higher for the two most critical damages (DAM-2 and DAM-4) rather than less severe cases (DAM-1 and DAM-3), where there is only for Area 5 an effective survivability change. Such a matter confirms the trend already shown for $N_r = 10$ by Mauro and Vassalos (2022a) and is essentially due to the different coupling between the bi-dimensional capsize band and the wave occurrences across the sea Areas. However, the survivability level also influences the oscillations of s_{A_χ} with N_r, clearly observable in the given figure. Once survivability is between 0.9 and 1.0, the differences across consecutive iterations are relatively small, regardless of the sea Area of interest, as it is observable, especially for DAM-1 and DAM-3.

As mentioned, Fig. 16 also shows the variation of Δs_{A_χ} with N_r, which is visible in the lower set of graphs adopting, to improve readability, a logarithmic representation on the y-axis. The variations of Δs_{A_χ} across consecutive repetitions present significant oscillations for all four damage cases and in all three reference sea Areas. However, the survivability value seems to influence the oscillation magnitude,
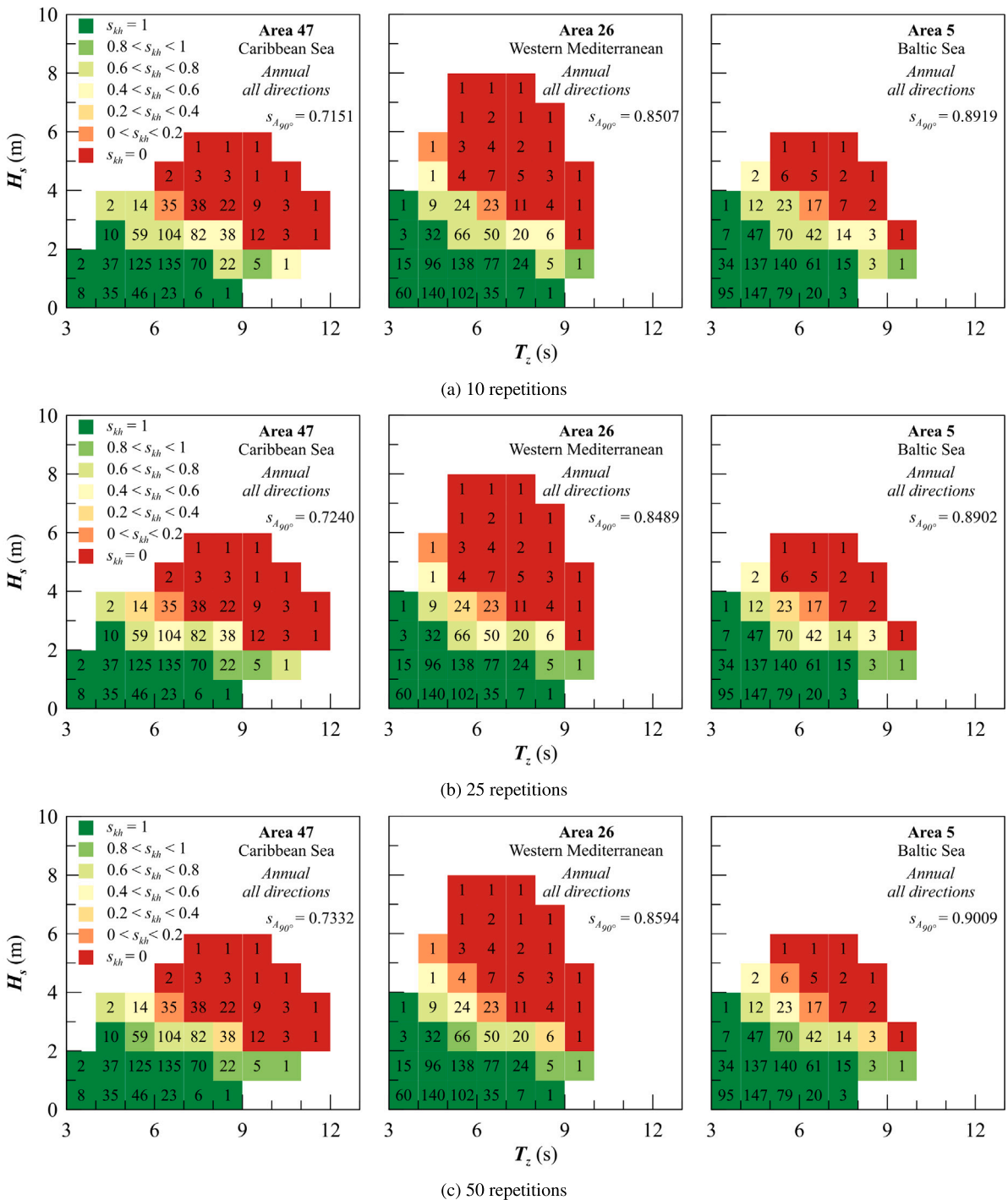
Fig. 13. DAM-2 survivability in the three selected sea areas considering 10 (a), 25 (b) and 50 (c) repetitions.

as the Δs_{A_χ} values for Area 5 (the one presenting higher survivability levels) are lower than the other two sea Areas. The individual damages DS for the same Areas confirms such a trend, with lower Δs_{A_χ} values for DAM-1 and DAM-3 than for DAM-2 and DAM-4. Nevertheless, the main scope of the Δs_{A_χ} analysis is to identify a suitable number of repetitions to achieve a reasonable convergence threshold for s_{A_χ}. To this end, the Δs_{A_χ} graphs in Fig. 16 also report the convergence thresholds corresponding to one day and five days a year. Observing the Δs_{A_χ} curves for all damages and sea Areas, after ten repetitions, all the variations are below the five days a year threshold. That means the assumption of $N_r = 10$ of the initial reference studies (Spanos and Papanikolaou, 2014; Mauro and Vassalos, 2022a) give a confidence of

at most about one weak on the detected survivability levels for the analysed cases. When the survivability level is high (e.g. between 0.9 and 1.0 as for Area 5, or close to 1.0 in general), the threshold of 1 day a year is satisfied also with ten repetitions.

However, when the s_{A_χ} value is lower than 0.9, thus representative of a more critical damage case, ten repetitions appear to be few to reach a threshold close to 1 day a year. Assuming that the convergence threshold of 1 or 2 days a year is a good approximation for the scatter diagram approach to damage stability, ensuring a reasonable balance between accuracy and amount of calculations, 20 repetitions are a suitable minimum amount of repetitions for a single cell. Therefore, after this sensitivity analysis, $N_r = 20$ is the suggested minimum
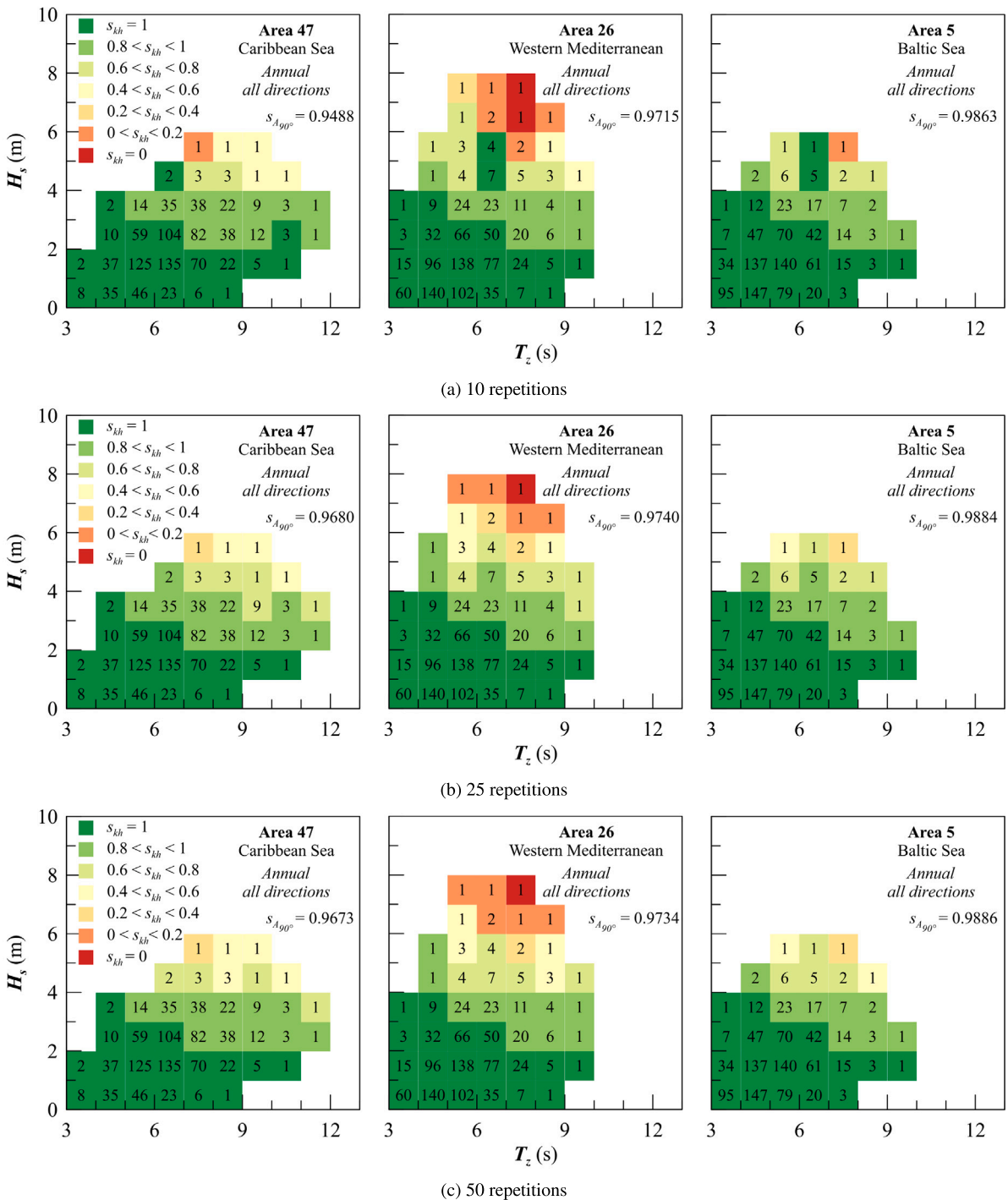
Fig. 14. DAM-3 survivability in the three selected sea areas considering 10 (a), 25 (b) and 50 (c) repetitions.

amount of repetitions for each environmental condition of interest. To reach a higher convergence level, the number of consecutive repetitions increases, as it is for the operability evaluation of a ship (Mauro and Nabergoj, 2022), where values of 1 hour a year are used. However, such restrictive thresholds are, for the moment, too accurate for the assumptions of state-of-the-art damage stability calculations.

According to the sensitivity analysis results, all the survivability analyses reported in the paper adopt $N_r = 20$, which is higher than the N_r adopted in damage stability studies available in the literature (Ruponen et al., 2019; Mauro and Vassalos, 2022a; Spanos and Papanikolaou, 2012; Cichowicz et al., 2016; Mauro et al., 2022b, 2023) but in line

with recent benchmarking studies in irregular waves (Ruponen et al., 2022a,b).

5.2. Effect of heading

After determining a minimum number of repetitions suitable for survivability calculation on a single condition, this Section discusses the effect of heading on the capsize rates. The sensitivity study highlighted no substantial differences between collisions and side-groundings cases; therefore, the present investigation on the heading effect considers DAM-1 and DAM-2 only.
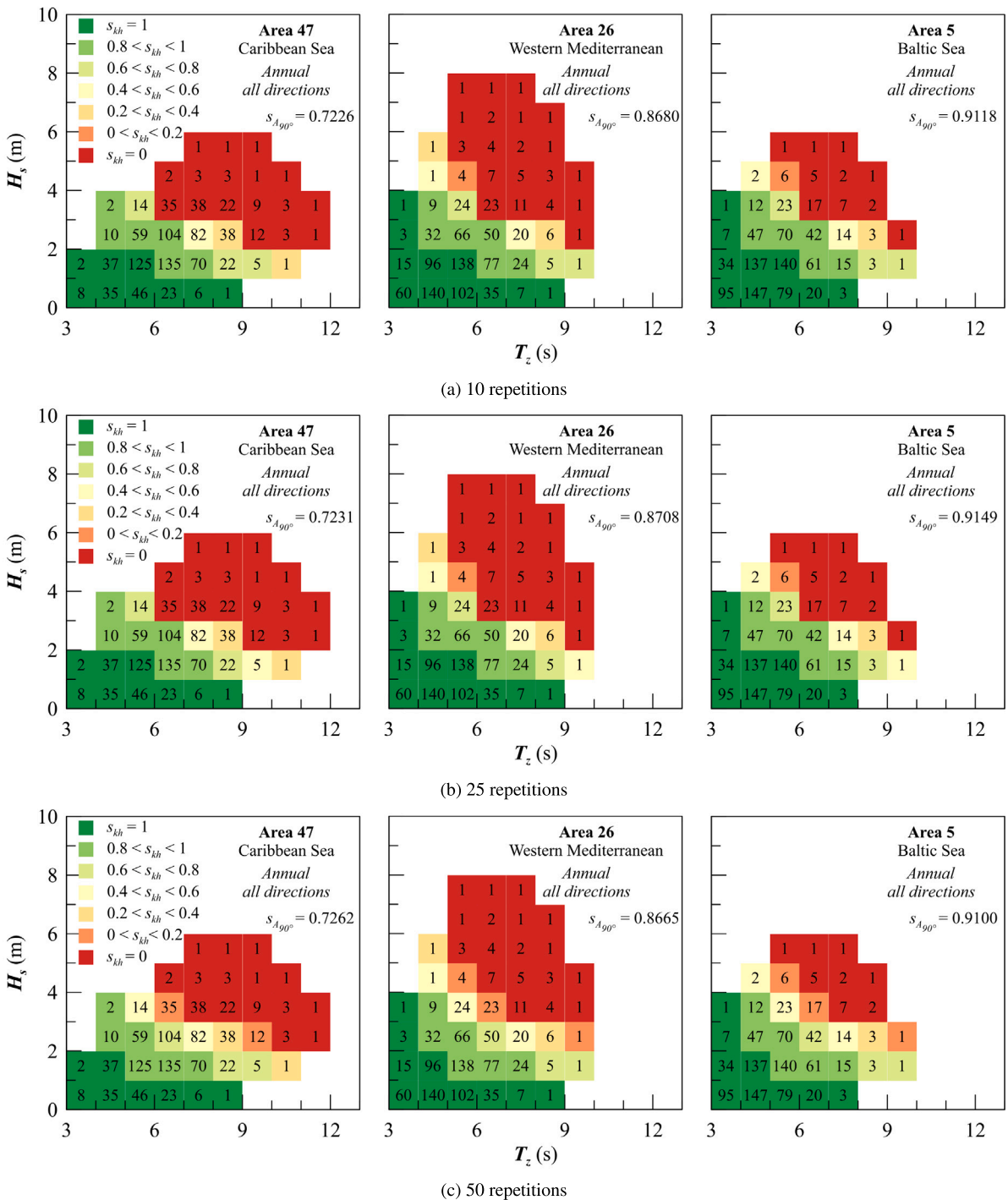
Fig. 15. DAM-4 survivability in the three selected sea areas considering 10 (a), 25 (b) and 50 (c) repetitions.

The time-domain simulations at different headings do not consider the yaw motion; thus solving a 4 DOF system of equations as it is for the conventional simulations at $\chi = 90$ degrees. The Section reports in graphical and tabular form the cells survivability s_{kh} and the Area s_{A_χ}.

As mentioned in Section 2, the survivability calculations consider only the beam sea encounter condition $\chi = 90$ or 270 degrees, according to the side of the damage. Such an initial setting reflects the concept of performing a simulation on the possible worst condition the vessel may encounter, thus being on the *safe side*. Here, the simulations evaluate the survivability in the sea area by changing the heading around the intrinsically supposed worst condition. 60 and 120 degrees are the first heading conditions investigated for both collision damages.

Figs. 17 and 18 show the results for the three reference scatter diagrams, adopting an analogue representation of Figures from 12 to 15 in the previous Section. Fig. 17 shows the survivability in the three sea areas for damage DAM-1 at heading 60 degrees (Fig. 17(a)), 90 degrees (Fig. 17(b)) and 120 degrees (Fig. 17(c)). All cases consider $N_r = 20$; thus, the 90 degrees condition does not match the solutions provided in Fig. 12. The reported local cells survivabilities s_{kh} highlight that there is a difference between the safe and unsafe combinations of H_s and T_z at different headings. Also, the area survivability levels confirm such a difference, registering higher S_{A_χ} for $\chi = 90$ degrees and comparable values for $\chi = 60$ and 120 degrees. Of course, the differences between the individual areas remain due to the already described local wave
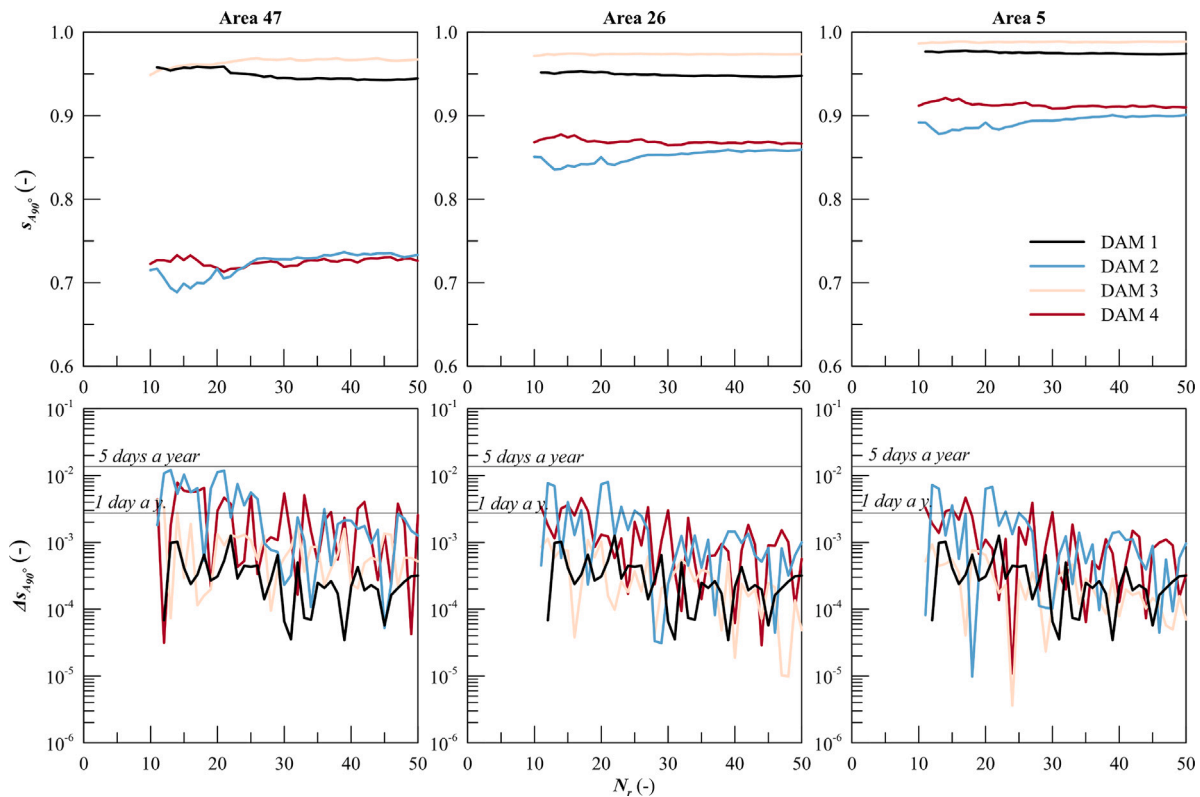
Fig. 16. Survivability (*top*) and variations (*bottom*) as a function of N_r for the four damages in the three reference sea areas.

statistics. Looking more in detail at the cells s_{kh} between 60 and 120 degrees, the critical values with $s_{kh} > 0$ appear for higher couples $H_s - T_z$ for $\chi = 120$ rather than $\chi = 60$ degrees. However, the occurrence of the cells where the highest differences are present is statistically insignificant, leading to almost equal area survivabilities.

Fig. 18 shows the survivability in the three sea areas for damage DAM-2 at heading 60 degrees (Fig. 18(a)), 90 degrees (Fig. 18(b)) and 120 degrees (Fig. 18(c)), considering 20 repetitions per cell simulation. As for DAM-1, the differences among the headings are visible in the cell survivability s_{kh} values, confirming the lower survivability level for the beam sea condition. However, the survivability in the three reference areas is lower for $\chi = 60$ degrees instead of 120, opposing the trend shown by DAM-1. Being DAM-2 a most severe case than DAM-1, as it is representative of a two-failure case damage (see Section 4), the area survivability levels in the three areas is lower than DAM-1, and the differences in S_{A_χ} between headings are higher too. A reason for the different trend with the encounter headings between the two damages is the location of the damage. DAM-1 stands on the aft shoulder of the ship, whilst DAM-2 is between the midship and fore shoulder. Such a matter may justify the higher impact on survivability of 60 degrees for DAM-2 and 120 deg for DAM-1, thus conditions where the damage is facing more directly the incoming wave system. Besides the damage location, also the internal layout and the consequent coupling with trim and flow-mass entering the ship emphasise the differences in damage severity. In any case, the worst state remains 90 degrees; however, additional calculations have been carried out on DAM-2 (the worst damage case), considering intermediate headings between 60 and 120 degrees. The supplementary simulations confirm that $\chi = 90$ degrees is the worst case for that damage, as the survivability decreases while reaching the beam sea conditions. Figs. 19(a) and 19(b) graphically report the trend of the above-described considerations on S_{A_χ} survivability and headings. The representation also includes the two-day-a-year threshold, highlighting how S_{A_χ} differences among the χ are outside the threshold value. Not the same falls for the different S_{A_χ} between the sea areas on the same damages, whereas for DAM-1,

Table 5
s_{A_χ} values at different N_r for the four analysed damage cases in the three reference sea areas.

χ (deg)	$p(\chi)$ (–)	Area 47	Area 26	Area 5
0	0.042	0.8870	0.9660	0.9853
30	0.083	0.8768	0.9593	0.9822
60	0.083	0.8010	0.9195	0.9574
75	0.000	0.7642	0.8832	0.9231
90	0.083	0.7123	0.8504	0.8934
115	0.000	0.8433	0.9361	0.9678
120	0.083	0.8787	0.9521	0.9781
150	0.083	0.9414	0.9786	0.9929
180	0.083	0.9436	0.9812	0.9943
210	0.083	0.9637	0.9839	0.9962
240	0.083	0.9303	0.9681	0.9881
270	0.083	0.8533	0.9198	0.9535
300	0.083	0.8244	0.9302	0.9642
330	0.083	0.8811	0.9615	0.9838
360	0.042	0.8870	0.9660	0.9853
S_A (–)		0.8744	0.9476	0.9724

the final S_{A_χ} for Areas 47 and 26 lay inside the thresholds. Therefore, the severity of DAM-1 for the given heading is equivalent between the two areas without a statistic-consistent difference.

The survivability level S_A of a damage case in a sea area, according to Eq. (23), considers the presence of multiple headings. Therefore, a complete survey should investigate a broader set of encounter angles. To this end, an additional set of calculations has been carried out, systematically changing the heading χ from 0 to 360 in steps of 30 degrees. As the investigation around $\chi = 90$ degrees showed that DAM-2 presents more S_{A_χ} variations across the headings, this collision case is the best candidate for additional simulations.

Fig. 20 shows the obtained S_{A_χ} for the different headings in polar form, also keeping the intermediate angles around 90 degrees. It is observable that the trend of the S_{A_χ} polar plots is similar between the sea areas, confirming the higher severity for 90 degrees. As expectable,

(a) Heading 60 degrees
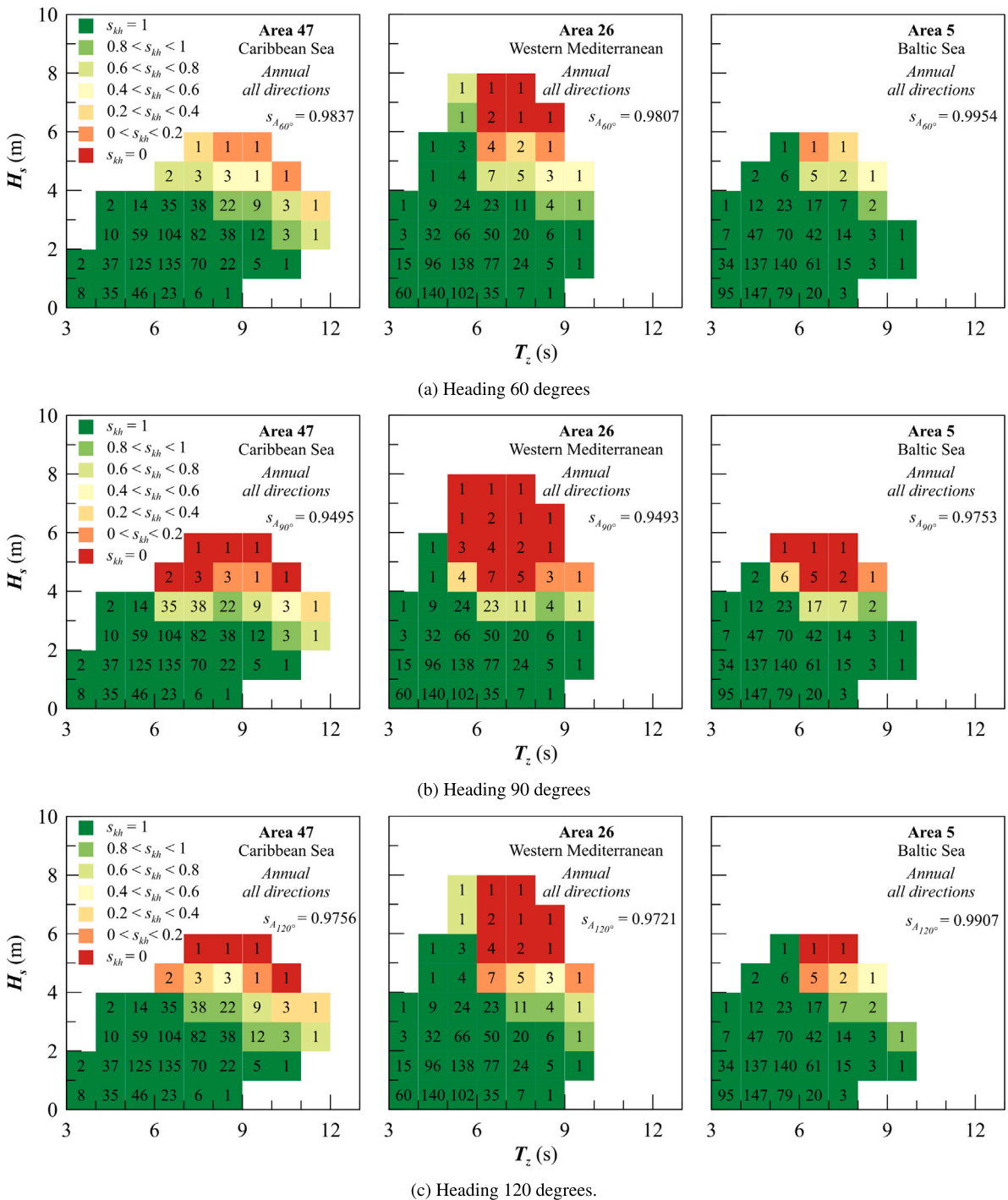

(b) Heading 90 degrees

(c) Heading 120 degrees.

Fig. 17. DAM-1 survivability in the three selected sea areas considering a heading χ of 60 (a), 90 (b) and 120 (c) degrees on 20 repetitions.

the survivability of encounter conditions changes with the headings, being higher for χ angles where the damage is not directly facing the breach. Therefore, the resulting capability plot is not symmetric between 0 and 180 degrees nor between 90 and 270 degrees. Table 5 reports the survivability level S_{A_χ} for all the analysed headings, giving the weights used to obtain the final global survivability S_A. In such a case, only the 30 degrees steps contribute to the S_A values for the three reference sea areas, considering homogeneous weights among headings. The obtained survivability levels S_A are different for each sea area and, of course, are higher than the survivability level for heading

90 degrees only, which means the traditionally adopted encounter conditions. The ranking between the sea areas remains the same as the 90 degrees condition, confirming Area 47 as the most severe for the considered damage case.

The evaluation of S_A according to Eq. (23) and considering 12 headings requires the execution of 52 simulations repeated 20 times (or with an alternative N_r). The execution of such a high number of calculations for a damage case (12,480 in total) suggests that, without having a dedicated calculation cluster for damage stability, the complete scatter diagram approach is suitable only for selected damage
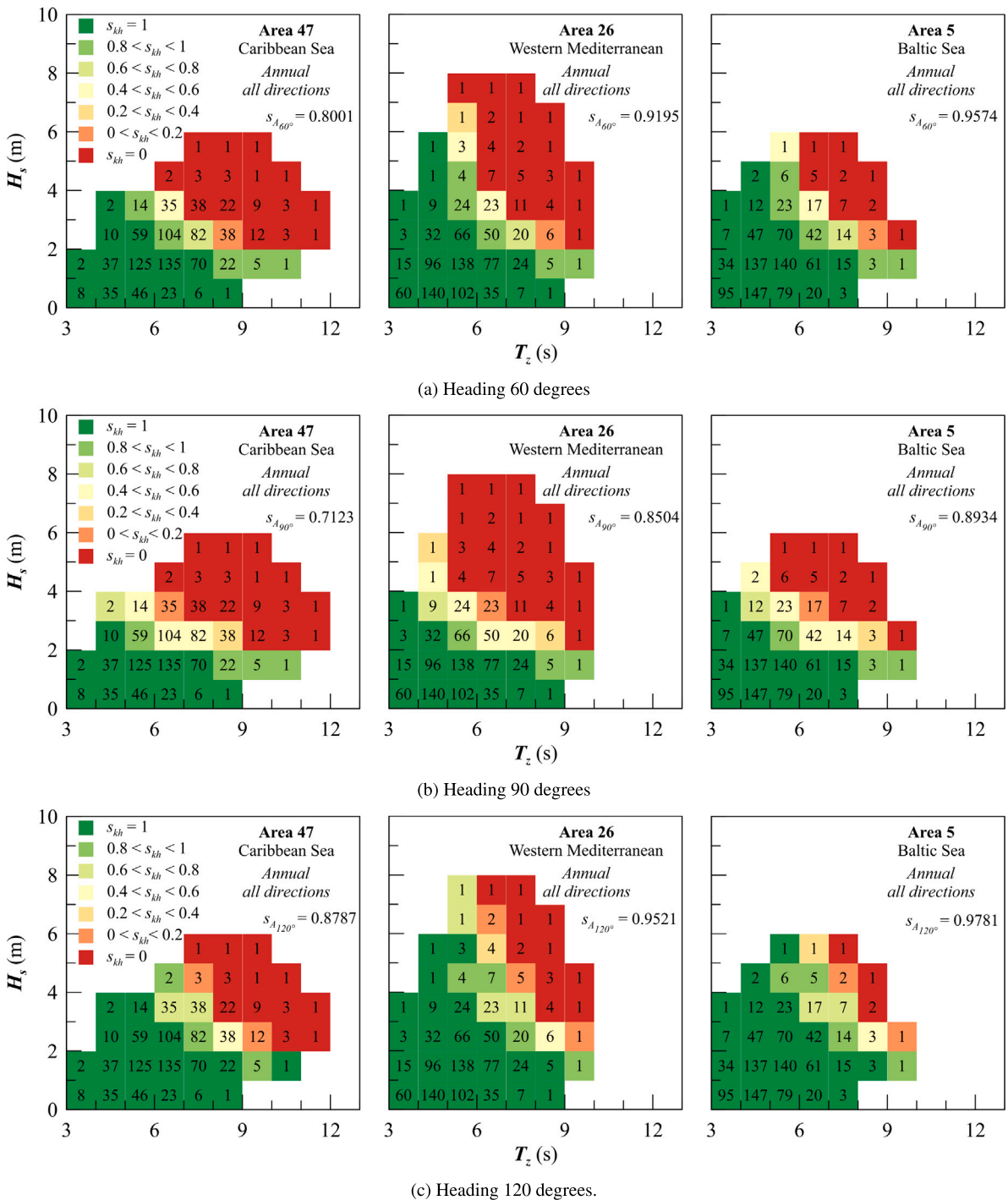
(a) Heading 60 degrees

(b) Heading 90 degrees

(c) Heading 120 degrees.

Fig. 18. DAM-2 survivability in the three selected sea areas considering a heading χ of 60 (a), 90 (b) and 120 (c) degrees on 20 repetitions.

cases filtered from a broader initial set of dynamic simulations aimed to identify critical damages.

5.3. Concluding remarks

The current work presents alternative methodologies for evaluating the survivability of a damage case in an irregular sea environment. The previous sections focus on the methodology, calculation settings and results obtained employing these newly introduced environmental modelling. However, here and in the preliminary study from the literature (Mauro and Vassalos, 2022a), a comparison between survivability

levels obtained with the conventional methods and the proposed ones is still missing.

Table 6 presents the obtained results adopting the conventional survivability s_{H_s}, based on the application of Eq. (9), the area-specific survivability S_{A_χ} for $\chi = 90$ degrees (Eq. (24)) with fixed and free yaw, and the S_A based on Eq. (23). For a fair comparison, all the reported data refer to $N_r = 20$ repetitions for simulations of 30 minutes of exposure time. As mentioned during the individual analyses, a complete comparison between all the tested options is available only for DAM-2; however, the results for other damages highlight the main differences between a conventional and a scatter diagram approach. The table reports the survivability values and the relative comparison between
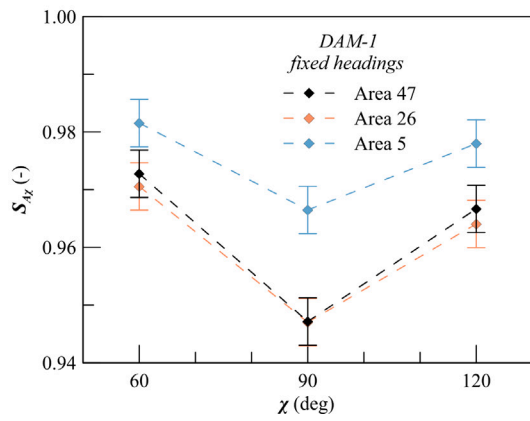
(a) DAM-1 survivability level.
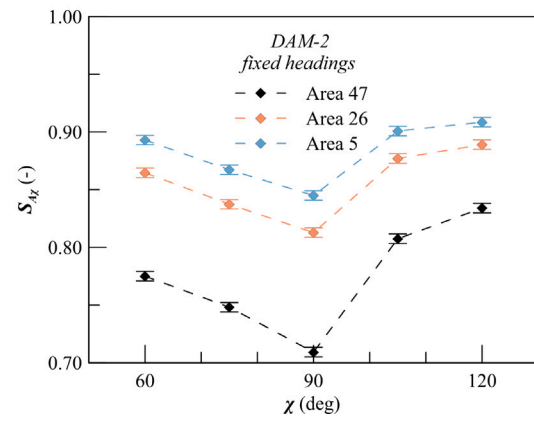
(b) DAM-2 survivability level.

Fig. 19. Survivability levels for DAM-1 and DAM-2 with 2 days uncertainty thresholds considering fixed heading simulations.
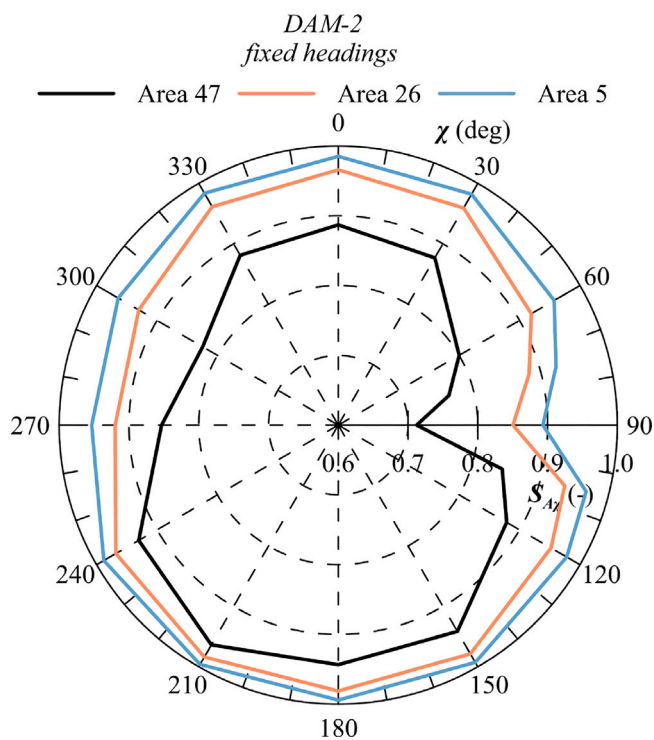

Fig. 20. Polar representation of survivability S_{A_χ} for DAM-2 for the three reference sea areas.

Table 6
Survivability for the four analysed reference damages according to different methods and percentage differences δs (in the brackets).

Survivability		DAM-1	DAM-2	DAM-3	DAM-4
s_{H_s} Eq. (9)		0.8417	0.6067	0.9073	0.6621
$s_{A_{90°}}$ Eq. (23)	Area 47	0.9495 (+12.81)	0.7123 (+17.41)	0.9623 (+6.06)	0.7177 (+8.40)
	Area 26	0.9493 (+12.78)	0.8504 (+40.16)	0.9735 (+7.30)	0.8685 (+31.17)
	Area 5	0.9753 (+15.87)	0.8934 (+47.26)	0.9878 (+8.87)	0.9128 (+37.86)
s_A Eq. (22)	Area 47	– (–)	0.8744 (+44.12)	– (–)	– (–)
	Area 26	– (–)	0.9474 (+56.16)	– (–)	– (–)
	Area 5	– (–)	0.9724 (+60.27)	– (–)	– (–)

conventional and alternative survivability measured through the index δs having the following form:

$$\delta s\,(\%) = 100\frac{s_{new} - s_{H_s}}{s_{H_s}} \text{ with } s_{new} \in \left(s_A, s_{A_\chi}\right) \qquad (26)$$

The reference survivability s_{H_s} used in the formulation is already a function of a higher number of repetitions than the standard used in conventional damage stability simulations, but, as mentioned, $N_r = 20$ is the standard of this study after the sensitivity analysis. Therefore, the relative differences obtained by employing the five or ten repetitions suggested by other studies may differ from the reported values in Table 6. However, the provided comparison is representative of calculations having the same confidence on the final survivability level and, therefore, more reliable than mixing values with different convergence thresholds.

The results listed in the table summarise the differences between the alternative methods already stressed in the previous sections, adding a comparative variation with state-of-the-art predictions. All the proposed alternative methods for the survivability evaluation in a realistic sea environment produce higher survivability values than conventional simulations. The δs increases range from 6 to almost 60% of the s_{H_s} values among the damages, stressing the dependency on the sea areas, damage severity and analysis type. Less severe is the damage case, and lower is the difference in δs changing the analysis type. On the contrary, an opposite trend correlates with sea areas, where less severe wind-wave occurrences generate a higher advantage in terms of gained survivability. Concerning the proposed methods, the total area survivability s_A (Eq. (23)) has the highest increase compared to s_{H_s}, even though it has been tested only for DAM-2. In any case, the number of calculations needed to perform the survivability analysis in specific sea states and encounter conditions significantly increases compared to standard damage stability assessments, also by considering a reduced number of repetitions instead of $N_r = 20$ coming from the sensitivity study. It is then advisable to use these more detailed and advanced predictions only for a significant set of critical damages, for forensic analyses or for demonstrating the effectiveness of an internal layout in severe conditions. An alternative application of the proposed methodologies requires an improvement in the calculation time of the damage stability codes and a simulation-oriented transition of designers to the damage stability problem (Mauro et al., 2023), giving more space to complex simulation in the design process of passenger ships.

The last consideration concerns the suggested number of repetitions of irregular wave cases. The sensitivity study focuses on the repetition

Table 7
Time to capsize mean values at different N_r for the four damage cases in a given environmental condition (H_s=3.5 m, T_z=6.5 s and χ=90 deg).

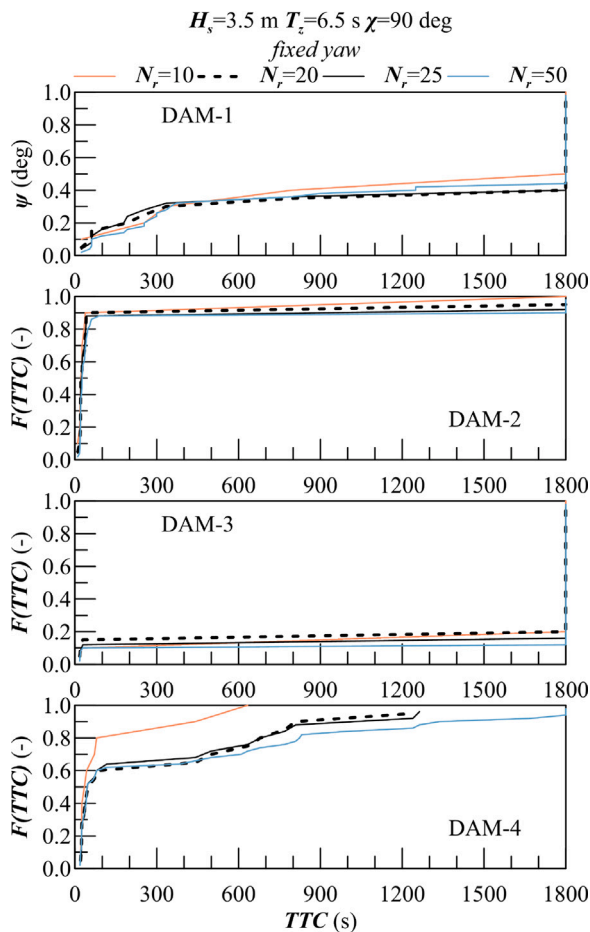| N_r	Mean TTC (s)			
	DAM-1	DAM-2	DAM-3	DAM-4
10	1220.8	201.1	1622.8	139.7
20	1256.1	203.6	1533.2	339.4
25	1232.0	238.5	1586.6	333.8
50	1202.4	242.4	1622.1	427.5

Fig. 21. Time to capsize TTC cumulative distributions at different N_r for the four sample damages.

needed to reach a given confidence threshold in the survivability level. However, time-domain simulations provide additional outputs relevant to the interpretation/analysis of damage stability of ships, such as, for example, the time to capsize TTC (Cichowicz et al., 2016; Spanos and Papanikolaou, 2014).TTC is extremely relevant for the determination of the risk assessment of the ship (Vassalos et al., 2022d), as it contributes to the estimation of the fatalities occurring after an accident in combination with the results of evacuation analyses. Then, accurate estimation of TTC is of utmost importance for risk analyses. As an example, Table 7 reports the mean TTC values extrapolated from simulations performed in H_s=3.5 m and T_z=6.5 s for the heading of 90 degrees with fixed yaw. The values refer to different repetitions, highlighting that the mean value of TTC is not reaching a clear trend for convergence between the 50 repetitions. The mean value for TTC is the significant measure of TTC used in the literature (Cichowicz et al., 2016); however, as recognisable in Fig. 21, the TTC may have a cumulative distribution where the mean TTC is less significant than other statistical orders to

define an extreme event. In any case, Fig. 21 highlights that the cumulative TTC distributions do not reach convergence after 50 repetitions for the reported cases. Therefore, for performing detailed forensic analyses, it is advisable to increase the number of repetitions, but this should require dedicated analyses and studies. In addition, despite the fact that PROTEUS3 software is capable of reproduce model experiments on damaged large passenger vessels (Ruponen et al., 2022b), there are still concerns about the code reliability for severe sea states (i.e. simulations with H_s higher than 4.5–5.0 m). Such a matter is crucial once quantities like TTC needs to be evaluated, as the associated uncertainties increases as indicated by benchmarking activities. Furthermore, there is still not available measurement for ship survivability as a function of vessel heading. Even though the study remains purely numerical, it is still a good starting point to promote enhanced analyses of damaged stability, with emphasis on more realistic operational environmental conditions.

As a last comment, all the calculations performed in this study refer to an environmental modelling which refers to a long-crested sea. The obtained results are valid for this condition; however, it could be of interest evaluating the survivability of the damaged ship also for short-crested seas, employing a spreading function for the wave spectra, and checking whether the survivability and TTC remains present different peculiarities.

6. Conclusions

The present work proposes alternative methods to conventional damage stability analyses for performing survivability evaluation of critical damage cases in a site-specific irregular sea environment. The adopted methods abandon the standard definition of the damaged ship wave environment employing the significant wave height only in favour of a bi-dimensional characterisation, including the zero-crossing period. Adopting a continuous bivariate wave distribution or a scattered approach (scatter diagram) allows for avoiding statistical incongruences highlighted for the conventional wave height distribution employed in damage stability. Sensitivity analysis identifies the minimum number of repetitions needed to gain a satisfactory level of convergence for survivability. With the selected number of repetitions, the application of operativity calculation in different sea areas and headings highlight the different severities of the same damage in distinct operational areas, with a consistent decrease in damage severity compared to conventional analyses.

The main considerations and way forward from additional research can be summarised in the following points:

- *Wave distribution*: despite the adoption of a scatter diagram approach, with the consequent adoption of site-specific bivariate wave distributions, dedicated work needs to be done for an appropriate an consistent formal description of the H_s distribution. As highlighted in the paper, the distributions in use in the damage stability assessment does not represent a probability space and should be reformulated to provide a reliable instrument for standard assessments.
- *Scatter approach*: the survivability evaluation on a given set of wave parameter combination allows for detecting the damage severity in operational areas specific for passenger ships. The evaluation of more than one single encounter condition contributes to the detection of higher survivability levels compared to standard survivability assessment. The adoption of a scatter diagram approach implies the execution of a higher number of calculations compared to conventional analyses; however, such an approach provides more insight in the identification of critical conditions. An effective and capillary application of the proposed methods in the damage stability assessment requires the improvement of the computational performances of state-of-the-art damage stability codes. Furthermore, benchmarking has been performed, nowadays, for beam seas condition only. Even though

the code PROTEUS3 shows a good agreement with the model tests in irregular waves, a verification is needed for the software capability in different heading conditions. Thus, it is highly recommended to promote further benchmarking studies on damaged ship survivability for more realistic operational conditions.

- *Number of repetitions*: the sensitivity analysis performed highlights that 20 repetitions of an irregular wave condition may be sufficient to grant a convergence threshold of 2 days in a year. Such a N_r can be enough for survivability evaluation but appears to be not sufficient for other quantities of interest as the time to capsize, suggesting the need for additional investigation on that topic.

The application and in-depth analyses of the highlighted points will further increase the information available on vessel survivability since the early ship design process. Such a matter will strongly contribute towards the transition from prescriptive approaches to fully direct calculations to assess the damage stability problem in the design of passenger ships.

CRediT authorship contribution statement

Francesco Mauro: Conceptualization, Methodology, Investigation, Calculation, Software, Writing – original draft, Writing – review & editing. **Dracos Vassalos:** Writing – review & editing, Supervision.

Declaration of competing interest

The authors declare that they have no known competing financial interests or personal relationships that could have appeared to influence the work reported in this paper.

Data availability

Data will be made available on request.

References

Atzampos, G., 2019. A Holistic Approach to Damage Survivability Assessment of Large Passenger Ships (Ph.D. thesis). University of Strathclyde.

Bulian, G., Cardinale, M., Dafermos, G., Lindroth, D., Ruponen, P., Zaraphonitis, G., 2020. Probabilistic assessment of damaged survivability of passenger ships in case of groundings or contact. Ocean Eng. 218, 107396.

Bulian, G., Lindroth, D., Ruponen, P., Zaraphonitis, G., 2016. Probabilistic assessment of damaged ship survivability in case of grounding: Development of a direct non-zonal approach. Ocean Eng. 120, 331–338.

Carette, N., van Walree, F., 2019. In: Belenky, V., Spyrou, K., van Walree, F., Almeida Santos Neves, M., Umeda, N. (Eds.), Contemporary Ideas on Ship Stability. Fluid Mechanics and Its Applications, Vol. 119. Springer, Cham., pp. 213–222.

Cichowicz, J., Tsakalakis, N., Vassalos, D., Jasionowski, A., 2016. Damage survivability of passenger ships - re-engineering the safety factor. Safety 2 (1), 4.

DNV, 2014. DNV RP C205 Environmental Conditions and Environmental Loads. Technical Report, Det Norske Veritas.

eSAFE, 2017-2018. Enhanced stability after a flooding event. A joint industry project on Damage Stability for Cruise Ships.

FLARE, 2018-2022. Flooding accident response. EU Funded Research Project, Contract No.: 814753, Website: www.flare-project.eu.

Guarin, L., Paterson, D., Murphy, A., Vassalos, D., Mauro, F., 2021. D5.8 Dynamic Vulnerability Screening. Technical Report, WP5 Project FLARE.

Gutsch, M., Steen, S., Sprenger, F., 2020. Operability robustness index as seakeeping performance criterion for offshore vessels. Ocean Eng. 217, 107931.

HARDER, 2000-2003. Harmonization of rules and design rational. EU Funded Research Project, FP5, DG XII-BRITE.

Hasselmann, K., Olbers, D., 1973. Measurements of wind-wave growth and swell decay during the joint north sea wave project (JONSWAP). Ergänzung Zur Deut. Hydrogr. Z. 8 (12), 1–95.

Hogben, N., Dacunha, N., Olliver, G., 1986. Global Wave Statistics. British Maritime Technology Limited.

IMO, 2009. SOLAS-International Convention for the Safety of Life at Sea. Technical Report, IMO, London, UK.

IMO, 2020. International Convention for the Safety of Life at Sea (SOLAS). Technical Report, IMO, Consolidated edition as of 2020.

Jasionowski, A., 2001. An Integrated Approach to Damage Ship Survivability Assessment (Ph.D. thesis). University of Strathclyde.

Jasionowski, A., 2009. Study of the Specific Damage Stability Parameters of Ro-Ro Passenger Vessels According to SOLAS 2009 Including Water on Deck Calculation. Technical Report, 2nd EMSA study on damage stability of RoPax vessels, Project No EMSA/OP/08/2009. Ship Stability Research Centre, University of Strathclyde.

Kwon, S., Chen, Q., Mermiris, G., Vassalos, D., 2019. In: Belenky, V., Spyrou, K., van Walree, F., Almeida Santos Neves, M., Umeda, N. (Eds.), Contemporary Ideas on Ship Stability. Fluid Mechanics and Its Applications, Vol. 119. Springer, Cham., pp. 753–771.

Luhmann, H., 2019. FLARE-D2.1 – Sample Ships - Overview. Technical Report, FLARE Project.

Luhmann, H., Bulian, G., Vassalos, D., Olufsen, O., Seglem, I., Pottgen, J., 2018. eSAFE-D4.3.2 – Executive summary. Technical Report, Joint Industry Project eSAFE - enhanced Stability After a Flooding Event – A joint industry project on Damage Stability for Cruise Ships.

Manderbacka, T., Themelis, N., Bačkalov, I., Boulougouris, E., Eliopoulou, E., Hashimoto, H., Konovessis, D., Leguen, J., Miguez Gonzalez, M., Rodriguez, C., Rosen, A., Ruponen, P., 2019. An overview of the current research on stability of ships and ocean vehicles: The STAB2018 perspective. Ocean Eng. 186, 106090.

Mauro, F., Nabergoj, R., 2022. A probabilistic approach for dynamic positioning capability and operability predictions. Ocean Eng. 262, 112250.

Mauro, F., Prpić-Oršić, J., 2020. Determination of a DP operability index for an offshore vessel in early design stage. Ocean Eng. 195, 106764.

Mauro, F., Vassalos, D., 2022a. An area-specific survivability assessment for passenger ships. In: 14th International Marine Design Conference, IMDC 2022, 26-30 June, Vancouver, Canada.

Mauro, F., Vassalos, D., 2022b. The influence of damage breach sampling process on the direct assessment of ship survivability. Ocean Eng. 250, 111008.

Mauro, F., Vassalos, D., Paterson, D., 2022a. Critical damages identification in a multi-level damage stability assessment framework for passenger ships. Reliab. Eng. Syst. Saf. 228, 108802.

Mauro, F., Vassalos, D., Paterson, D., Boulougouris, E., 2022b. Exploring smart methodologies for critical flooding scenarios detection in the damage stability assessment of passenger ships. Ocean Eng. 262, 112289.

Mauro, F., Vassalos, D., Paterson, D., Boulougouris, E., 2023. Evolution of ship damage stability assessment—Transitioning designers to direct numerical simulations. Ocean Eng. 268, 113387.

Papanikolaou, A., 2007. Review of damage stability of ships - recent developments and trends. In: 10th International Symposium on Practical Design of Ships and Other Floating Structures, PRADS 2007, Vol. 1. pp. 497–509.

Papanikolaou, A., Hamman, R., Lee, B., Mains, C., Olufsen, O., Vassalos, D., Zaraphonitis, G., 2013. GOALDS: Goal based damage ship stability and safety standards. Accid. Anal. Prev. 60, 353–365.

Pawlowski, M., 2004. Subdivision and Damaged Stability of Ships. Euro-MTEC book series, Gdansk, Poland.

Pierson, W., Moskowitz, L., 1963. A proposed Spectral Form for Fully Developed Wind Seas Based on the Similarity Theory od S.A. Kitagorodski. Technical Report, U.S. Naval Oceanographic Office, C-62306-1042.

Ruponen, P., Lindroth, D., Routi, A., Aartovaara, M., 2019. Simulation-based analysis method for damage survivability of passenger ships. Ship Technol. Res. 66, 180–192.

Ruponen, P., Valanto, P., Acanfora, M., Dankowski, H., Lee, G., Mauro, F., Murphy, A., Rosano, G., van't Veer, R., 2022a. Results of an international benchmark study on numerical simulation of flooding and motions of a damaged ropax ship. Appl. Ocean Res. 123, 103153.

Ruponen, P., van Basten-Batemburg, R., van't Veer, R., Bu, S., Dankowski, H., Lee, G., Mauro, F., Ruth, E., Tompuri, M., 2022b. International benchmark study on numerical simulation of flooding and motions of a damaged cruise ship. Appl. Ocean Res. in press.

Santos, T., Winkle, I., Guedes Soares, C., 2002. Time domain modelling of transient asymmetric flooding of Ro-Ro ships. Ocean Eng. 29 (6), 667–688.

Spanos, D., Papanikolaou, A., 2012. On the time dependance of survivability of ROPAX ships. J. Mar. Sci. Technol. 17, 40–46.

Spanos, D., Papanikolaou, A., 2014. On the time for abandonement of flooded passenger shipsdue to collision damages. J. Mar. Sci. Technol. 19, 327–337.

Tsakalakis, N., Cichowicz, J., Vassalos, D., 2010. The concept of the capsize band revisited. In: 11th International Ship Stability Workshop (ISSW 2010), Wageningen, the Netherlands.

van Basten-Batemburg, R., van't Veer, R., Valanto, P., 2020. Deliverable 4.2 – Model tests. Technical Report, FLARE Project.

Vanem, E., Rusas, S., Skjong, R., Olufsen, O., 2007. Collision damage stability of passenger ships: Holistic and risk-based approach. Int. Shipbuild. Prog. 54 (4), 323–337.

Vassalos, D., 2016. Damage survivability of cruise ships - evidence and conjecture. Ocean Eng. 121, 89–97.

Vassalos, D., 2022. The role of damaged ship dynamics in addressing the risk of flooding. Ship Offshore Struct. 17 (2), 279–303.

Vassalos, D., Mujeeb-Ahmed, M., Paterson, D., Mauro, F., Conti, F., 2022a. Probabilistic damage stability for passenger ships - the p-factor illusion and reality. J. Mar. Sci. Eng. 10 (3), 348.

Vassalos, D., Paterson, D., 2022. Towards unsinkabel ships. Ocean Eng. 232, 109096.

Vassalos, D., Paterson, D., Mauro, F., Atzampos, G., Assinder, P., Janicek, A., 2022b. High-expansion foam: A risk control option to increase passenger ship safety during flooding. Appl. Sci. (Switzerland) 12 (10), 4949.

Vassalos, D., Paterson, D., Mauro, F., Mujeeb-Ahmed, M., Boulougouris, E., 2022c. Process, methods and tools for ship damage stability and flooding risk assessment. Ocean Eng. 266, 113062.

Vassalos, D., Paterson, D., Mauro, F., Mujeeb-Ahmed, M., Murphy, A., Michalec, R., Boulougouris, E., 2022d. A multi-level approach to flooding risk estimation of passenger ships. In: SNAM 14th International Marine Design Conference, IMDC 2022. Vancouver, BC, Canada.

Ventikos, N., Papanikolaou, A., Louzis, K., Koimtzoglou, A., 2018. Statistical analysis and critical review of navigational accidents in adverse weather conditions. Ocean Eng. 163, 502–517.